

## **Climatology and trends of the Indian Ocean surface waves based on 39-year long ERA5 reanalysis data**

**Muhammed Naseef T<sup>1,2</sup>, Sanil Kumar V<sup>1\*</sup>**

<sup>1</sup>Ocean Engineering, CSIR-National Institute of Oceanography  
(Council of Scientific & Industrial Research),  
Dona Paula, Goa - 403 004 India

<sup>2</sup>Research Scholar, Bharathidasan University,  
Tiruchirappalli - 620023 Tamil Nadu, India

\*Corresponding author: Tel: 0091 832 2450 327 Fax: 0091 832 2450 602  
Email: sanil@nio.org

### **Abstract**

In this study, the wind and the surface waves in the Indian Ocean (IO) during 1979-2017 are studied based on the ECMWF ERA5 Reanalysis data. Long-term statistical analysis of extreme waves is carried out based on Generalised Extreme Value distribution using annual maxima and the spatial distribution of return levels for 50 and 100-years are studied. In general, the ERA5 significant wave height ( $H_s$ ) and maximum wave height ( $H_{max}$ ) show a good agreement with measured buoy data in the coastal (bias~0.29 m) and deep waters (bias~0.18 m). During the tropical cyclone, underestimation of  $H_s$  and  $H_{max}$  in the ERA5 data compared to buoy data is 2.7% and 1.4%, but in general the bias is large (~0.69 m). Swell domination is observed in larger regions of the IO, whereas wind-seas are comparable to swells in the Southern Ocean. The meridional wind speed largely influences the spatial pattern of  $H_s$  in the North IO. The stronger winds over the Southern Ocean play a major role in generating higher waves at higher latitudes. Maximum value of the 100-year return level for  $H_s$  in IO is 17.8 m, whereas highest value of the  $H_s$  is 16.7 m and  $H_{max}$  is 32.0 m. Severe wave events are common at 50-60° S and only during 25% of the time in a year,  $H_{max}$  is less than 5 m in this region. Ratio of the  $H_{max}$  to  $H_s$  varies from 1.46 to 2.3 with a mean value of 1.87. The 100-year return value of  $H_s$  changed by -4 to 5 m, when the length of the dataset is decreased from 39 years (1979-2017) to recent 20 years. On an average, from 1979 to 2017, the annual average  $H_{max}$  increased by 0.73 cm/year. In major areas of the IO, a clear decrease of the  $H_s$  is observed during 1991-2017, whereas during 1979-2017, an increase in  $H_s$  is found.

**Key words:** Surface waves, reanalysis, Indian Ocean, ERA5, return period, climatology

## 1. Introduction

Ocean surface waves (wind-waves, hereinafter waves) play a major role in activity planning in the coastal zones and offshore areas (Tucker and Pitt, 2001). Information on waves are obtained through i) in situ measurements through buoys, ii) satellite-based altimeter measurements, iii) model datasets (Cavaleri and Sclavo, 2006). Direct observations from buoys remain the most reliable sources to study wave climate, but the data from the buoys are sparse and the spatial availability of the data is limited and previous studies show that changes to the buoy hulls and payloads over time cause discontinuities in the time series. The data from satellite altimeter covers large areas spatially, but the temporal resolution is poor compared to the buoy data since the satellite takes at least 10 days to return to the same point (Cooper and Forristall, 1997). The model datasets have good spatial and temporal coverage since they can be run at any spatial and temporal resolution. But the model datasets generally require validation for different geographical locations due to the difference in the regional wave climate. Data at low temporal resolution ( $> 3$  h) underestimate the maximum significant wave height ( $H_s$ ) by 6 to 26% during the monsoon and storm events (Anoop *et al.*, 2014). The climatological behaviour of waves is of interest to both the coastal engineering and scientific communities. Several global-scale wave climatologies have been developed using remotely sensed data (Young, 1999), visual observations (Gulev *et al.*, 2003), reanalysis data (Semedo *et al.*, 2011) and wind wave hindcasts (Cox and Swail, 2001; Liang *et al.*, 2019). The global distribution of  $H_s$  and the long-term wave height trends are estimated with the remotely sensed data by satellite radar altimetry (Izaguirre *et al.*, 2011; Young *et al.*, 2011).

Reanalysis provides a numerical description of the climate by combining altimeter data with models. Reanalysis wave data are now widely in wave climate studies in global and regional scales (Stopa and Cheung, 2014; Anoop *et al.*, 2015). ERA-Interim, the reanalysis data of the European Centre for Medium-Range Weather Forecasts (ECMWF) has 6-hourly temporal resolution and 1 deg spatial resolution (Dee *et al.*, 2011). Recently many researchers compared the ERA-Interim with the measured data. Stopa and Cheung (2014) observed that ERA-Interim data generally underestimate the wave height with lower standard deviations in comparison to observations, but it maintains slightly better error metrics. The ERA-Interim wave parameters are compared with the measured data in the North Indian Ocean (NIO) by Sanil Kumar and Naseef (2015) and Shanias and Sanil Kumar (2015) and observed that the high waves are largely underestimated by ERA-Interim. Naseef and Sanil Kumar (2017) observed that the 6-hourly interval data tend to miss high values of  $H_s$ , and hence there is a significant difference in the 100-year return level  $H_s$  obtained compared to data at 0.5-hourly interval. ECMWF has released a new ECMWF climate reanalysis data, ERA5 to replace

ERA-Interim (Hersbach and Dee, 2016). ERA5 is the fifth generation of atmospheric reanalysis from ECMWF. ERA5 provides hourly estimates of a large number of atmospheric, land and oceanic climate variables and the data cover the Earth with a 31 km grid.

Extreme waves are responsible for the most extreme loadings on ocean vessels and offshore structures. All of the studies on wave climatology and long-term trend analysis based on models, reanalysis or satellite altimeter data describe the variations in the  $H_s$  and/or mean wave period and do not describe the maximum wave height (Semedo *et al.*, 2011; Vinoth and Young, 2011; Young *et al.*, 2011; Kumar *et al.*, 2013; Sandhya *et al.*, 2014; Amrutha *et al.*, 2016). For practical applications, it is required to know the maximum height of an individual wave ( $H_{max}$ ) in the oceans at a given place during a specific duration. Earlier  $H_{max}$  data is obtained only through site-specific measurements. The ERA5 data contain the information on  $H_{max}$  along with  $H_s$ .

Waves are a key consideration for design and operation of offshore facilities. Thus, waves with a certain return level (50 or 100-year) are required and the variations in the waves with certain return level due to the change in length of the time series have significant impacts on many industries. Return levels of  $H_s$  on a global scale from satellite altimetry data (Vinoth and Young, 2011) and modelled results (Caires and Sterl, 2005) have been estimated previously. But the studies related to change in return level for  $H_s$  due to reduction in data length is limited.

Indian Ocean (IO) is the third largest ocean with ~20% of the water on the Earth's surface and is surrounded by Asia in the north, Africa in the west, Australia in the east and the Southern Ocean (SO) and Antarctica on the south (Fig. 1). The average depth of IO is 3,890 m. The monsoon winds are the dominant feature of the NIO, which reverses its direction over an annual cycle and are an example of strong ocean-atmosphere interaction over basin scales (Schott and McCreary, 2001) and the wave heights are much higher during the monsoon period (June-September) compared to rest of the year (Kumar *et al.*, 2014). Similarly, cyclonic storms are formed in NIO and the impact of the cyclonic storm is higher in the Bay of Bengal (BoB) than in the Arabian Sea (AS) and these events can cause higher wave heights for a shorter period of 3 to 5 days (Amrutha *et al.*, 2014). Large wave events generated from tropical cyclones (TCs) pose a significant threat to the coastal areas. Swells generated by TCs dominates the extreme wave climate of the BoB and the waves generated in the Southern Hemisphere characterize swell waves in the NIO (Amrutha *et al.*, 2017). In the AS, long well-developed waves from south and southwest are superimposed to the locally generated wind waves from west and northwest (Kumar *et al.*, 2014). During an annual cycle, the monsoon is the dominant mode of variability (92 % of the total variability) in the NIO (Anoop *et al.*, 2015). The

southeast trade winds in the south Indian Ocean (SIO) region between 10 and 30°S generate waves and it propagates into the NIO (Stopa and Cheung, 2014). Even though the SIO has severe wave climate due to the cyclones, most of the studies on climatology are as part of the global studies (Sterl *et al.*, 1998; Young, 1999; Cox and Swail, 2001; Caires and Sterl, 2005; Hemer *et al.*, 2010; Semedo *et al.*, 2011; Lecacheux *et al.*, 2012; Zheng and Li, 2017; Liang *et al.*, 2019; Young and Ribal, 2019). But none of the studies examined the climatology and trend of  $H_{\max}$  in the IO. It is now understood that the swells generated in the SO during intense SO extra-tropical cyclones propagate throughout the World's oceans (Hemer *et al.*, 2010). The general wave characteristics of the coastal waters of NIO are available in the literature (Anjali Nair and Sanil Kumar, 2016; Anjali Nair and Sanil Kumar, 2017; Glejin *et al.*, 2016; Sanil Kumar *et al.*, 2014; Patra *et al.*, 2016; Anjali Nair *et al.*, 2019).

Global climate change and its impact on the surface waves are discussed by various researchers (Fan *et al.*, 2013; Reguero *et al.*, 2019). Studies based on simulations of the Coupled Model Intercomparison Project (CMIP5) indicate an increasing trend in wave heights over the southern high latitudes and the tropics (Wang *et al.*, 2014). Different trends have been reported in various basins. The 109-year numerical hindcast showed an increase in the yearly-mean  $H_s$  in the North Atlantic Ocean (Bertin *et al.*, 2013). Castelle *et al.* (2018) showed that the winter-mean wave height increased significantly in the northeast Atlantic over the last seven decades. In the Italian seas during the second half of the 20th century, the winter averaged  $H_s$  had a statistically significant negative trend (Martucci *et al.*, 2010). Based on ERA-Interim over the period 1979-2012, no trend or a slightly negative trend in mean wave conditions are reported in the northern parts of the Pacific and Atlantic Oceans (Aarens *et al.*, 2015).

In the northern IO, historical satellite data (Patra and Bhaskaran, 2016) and reanalysis dataset (Zheng and Li, 2017) show increasing trend in annual mean  $H_s$ . Patra and Bhaskaran (2016) observed higher waves in the northern BoB during 2002-2012 than in the past decade. 18 years of altimeter data from 1993 to 2010 indicate that the variation in  $H_s$  in the IO is almost negligible (Kumar *et al.*, 2013). During 1979 to 2012, in the Central BoB, a weak decreasing trend is observed in annual mean  $H_s$  (Shanas and Sanil Kumar, 2015). The 23 year period (1985-2008) satellite altimeter data indicate a weak increase (0-0.25% of annual mean value) of  $H_s$  in NIO (Young *et al.*, 2011). During 1985-2008, in a small area of the central east coast of India Anoop *et al.* (2015) reported a negative trend of  $H_s$ , whereas in the same area Young *et al.* (2011) observed a small positive trend. In NIO, Aarnes *et al.* (2015) showed that there is an increase of  $H_s$  (0-0.5% of annual mean value per year) during 1979 - 1991 and during 1992 - 2012, there is a decrease (0-0.5%). In the central AS, a positive trend of 0.63 cm/year in the annual mean  $H_s$  is observed during 1996 to 2012

based on satellite altimeter data (Hithin *et al.*, 2015). Sanil Kumar *et al.* (2018) reported a statistically significant positive trend of 0.8 to 1.4 cm/year in annual mean  $H_s$  during 1998 to 2012 in the Indian shelf seas of NIO and the increasing trend is higher ( $\sim 0.7$  to 2.5 cm/year) during the Asian summer monsoon period (June-September). From 1998 to 2012, the average trend of annual mean wind speed is also positive and is higher ( $\sim 1.67$  cm/s/year) for the western shelf seas than that for eastern shelf seas ( $\sim 0.93$  cm/s/year) of India (Sanil Kumar *et al.*, 2018). Most of the studies related to historical changes in wave height report an increase in wave height in the past (Young *et al.*, 2011; Bertin *et al.*, 2013; Wang *et al.*, 2014), whereas other studies report nil or decreasing trends (Aarens *et al.*, 2015). In view of the contrasting trends reported in the past, it is important to re-examine the trends in the IO using the new dataset, i.e., ERA5.

In this study, the ERA5 wave height ( $H_s$  and  $H_{max}$ ), wave period (mean wave period and peak wave period) and wind speed data from 1979 to 2017 are used to describe its climatology and the ongoing trends. This 39 years period is more than the minimum period (30 years) for climate studies recommended by the World Meteorological Organization. The spatial distribution of monthly mean wind-sea and swell  $H_s$  are also examined. This is the first study which describes the climatology of  $H_{max}$  in the IO. Study also examines the difference in extreme waves estimated following the two commonly used distributions; Generalized Extreme Value (GEV) distribution and Generalized Pareto Distribution (GPD). The rest of the manuscript is as follow: the data and methods including the data resources and comparison with buoy data are described in section 2. Section 3 consists of results and discussion on the spatial and temporal variability of wind and wave climate and the long-term changes. Section 4 contains the conclusions.

## **2. Data and method**

### **2.1 ERA data**

ERA5 (Hersbach and Dee,2016) is the fifth generation atmospheric reanalyses of the global climate produced by ECMWF adding different characteristics to its predecessor, ERA-Interim. The ERA5 assimilation system uses the latest version of the Integrated Forecasting System (IFS Cycle 41r2) and modern parameterizations technique of earth process which allows to use variational bias scheme for not only satellite observation as in ERA-Interim but also for aircraft, ozone and surface pressure data. The ERA5 has improved spatio-temporal resolution compared to ERA-Interim as 6 hourly in ERA-Interim to hourly in ERA5 and from 79 km horizontal resolution with 60 vertical levels up to 0.1 hPa to 31 km with 137 levels up to 0.01 hPa in ERA5. The ERA5 data released so far covers the period from 1 January 1979 to near real time. A number of gridded variables are available

under ERA5, and here we focus on  $H_{\max}$ ,  $H_s$ , mean wave period ( $T_e$ ), peak period ( $T_p$ ) and the wind speed.

## 2.2 Buoy data

Since ERA5 assimilates only satellite altimetry, the comparison between reanalysis (which assimilates observations) and buoy data is carried out for the NIO and this comparison represents an independent source of information for validation. Table 1 provides the details of the locations and the periods of the data used for the comparison with ERA5 data, which includes the waves during the TC. The measured wave data using the moored directional waverider buoy in the coastal waters (1 off Ratnagiri, eastern AS and 1 off Gopalpur, northwestern BoB) and the moored Seatex buoy at 1 location in the central AS (AD02 15.00° N; 69.01° E) during February-December 2012 and 1 location in the central BoB (DS3 12.15° N; 90.75° E) during January-December 2003 are compared with ERA5 wave data. The wave data in the coastal areas are from measurements carried out by the National Institute of Oceanography (Council of Scientific & Industrial Research, Govt. of India) and the Indian National Centre for Ocean Information Services (Ministry of Earth Sciences, Govt. of India) as part of the project “Real-time wave data collection in the Indian waters for Coastal Ocean Forecast”. The deep water data are under the National Data Buoy Programme (Premkumar *et al.*, 2000). The directional waverider buoy measures surface gravity waves with heaves in the range of -20 and +20 m, with a resolution of 0.01 m in heaves and range of wave periods between 1.6 and 30 s. Accuracy of buoy measured significant wave height and period is 0.5% of measured value. Data stored continuously at 1.28 Hz interval, and the data for every 30 min are processed as one record (Datawell, 2009). The data analysis details are presented in Kumar *et al.* (2014). The  $H_s$  and the mean wave period ( $T_e$ ) were obtained from the spectral moments as  $H_s = 4\sqrt{m_0}$  and  $T_e = \frac{m_{-1}}{m_0}$ ,

where  $m_n$  is the nth order spectral moment and given by  $m_n = \int_0^\infty f^n S(f) df$ ,  $n=0$  and  $-1$ , and  $S(f)$  is the spectral energy density at frequency  $f$ . In the time domain, each individual wave is selected based on the zero-crossing method and the  $H_{\max}$  is computed. Spectral peak period ( $T_p$ ) is the inverse of the frequency at which the wave spectral density of the sea surface height reaches its maximum.  $T_p$  provides an indication of the source of waves;  $T_p$  will be small for locally generated wind-sea and swells will have longer wave periods. From the measured half-hour record, the records at 1-hr intervals are used for comparison with the ERA5 data.

### 2.3 Methodology

The trend and the statistical significance of trends in seasonal and annual wave height and wind speed are calculated using Mann-Kendall (MK) test (Sen, 1968, Burkey, 2006). The MK test is a non parametric way for identifying trends in the time series which is endorsed by the World Meteorological Organization (WMO) for hydro-meteorological trend assessments (Kundzewicz and Robson, 2010). A negative slope indicates  $H_s$  decrease and positive slope a  $H_s$  increase. Extreme waves, also referred to in terms of 39, 50 and 100-year return values (i.e., wave heights that are likely to be exceeded, on average, once in every 39, 50 and 100 years) are estimated from 39 years data using the commonly used methods in the Extreme Value Analysis (EVA), i.e., Generalized Extreme Value (GEV) distribution with annual maxima (AM) observations (Goda, 1992) and Generalized Pareto Distribution (GPD) with Peak Over Threshold (POT) approach (Coles et al., 2001). The difference in 39, 50 and 100-year return level value using data with 10 years (2008-2017), 15 years (2003-2017), 20 years (1998-2017), 25 years (1993-2017), 30 years (1988-2017) and 35 years (1983-2017) with 39 years (1979-2017) are estimated.

### 2.4 Comparison of ERA5 data with buoy data

Statistical parameters used for comparison of the ERA5 data with the measured wave data are the root-mean-square error (RMSE), bias and correlation coefficient (r) and are defined below. The bias is a statistical quantity that gives the average difference between the ERA5 and buoy data. A better fit of data between ERA5 and observations show a lower value of RMSE.

$$\text{RMSE} = \sqrt{\frac{1}{N} \sum_{i=1}^N (A_i - B_i)^2} \quad (1)$$

$$\text{Bias} = \frac{1}{N} \sum_{i=1}^N (A_i - B_i) \quad (2)$$

$$r = \frac{\sum_{i=1}^N |(A_i - \bar{A})(B_i - \bar{B})|}{\sqrt{\sum_{i=1}^N |(A_i - \bar{A})^2 (B_i - \bar{B})^2|}} \quad (3)$$

where N is the number of data points,  $A_i$  represents the ERA5 data,  $B_i$  is the data from the buoy and the over bar represents the mean value.

## Wave height

The measured and ERA5 wave parameters;  $H_s$ ,  $H_{max}$ ,  $T_e$  and  $T_p$  for two coastal stations (one in AS and another in BoB) for a year are compared in Fig. 2. The annual maximum value of  $H_{max}$  measured at Ratnagiri is 8.6 m, whereas that from the ERA5 is 7.6 m indicating an underestimation of ~12% in the ERA5  $H_{max}$  data (Fig. 2). Similarly, the annual maximum  $H_s$  measured is 5.2 m, whereas that from the ERA5 is 4.1 m. Monthly maximum  $H_s$  values are also underestimated in ERA5 by 9 to 39% with the maximum underestimation in March. Monthly maximum  $H_{max}$  values are underestimated in ERA5 by 2 to 34% (Fig. 2). The annual average value of  $H_s$  is close to buoy data with a negative bias of 0.04 m at Ratnagiri. In the western BoB, the maximum  $H_s$  values are overestimated 6% at Gopalpur (Fig. 2) and the annual average  $H_s$  values are overestimated by 3% (Table 2). The maximum  $H_{max}$  value is overestimated by 25% and the annual mean  $H_{max}$  value is overestimated in ERA5 by 28% at Gopalpur (Fig. 2). In the deep waters of AS, the annual mean  $H_s$  from ERA5 is 1.78 m and is close to the buoy data (1.71 m). The ERA5 has a negative bias of 0.07 m in the AS, whereas in the BoB, it has a positive bias of 0.18 m. The annual mean  $H_s$  in BoB from ERA5 is 1.80 m, whereas the buoy data has 1.61 m (Fig. 3). Since only mean wave period ( $T_{m02}$ ) is available from the deep water buoys and the wave period of ERA5 data is close to the  $T_e$ , large scatter is observed in case of wave period (Fig. 3).

Figure 4 presents time series of buoy measured and ERA5 and ERA-Interim wave parameters during TC Phailin. The maximum  $H_{max}$  measured is 13.13 m and is close to the value (12.95 m) from ERA5. Similarly, the maximum buoy measured  $H_s$  is 7.06 m and is close to the ERA5 value of 6.87 m, whereas the maximum  $H_s$  from ERA-Interim is 4.15 m indicating a large underestimation in ERA-Interim. It is worth noticing that the ERA5  $H_s$  is higher than in ERA-Interim. The underestimation in ERA5 during the TC Phailin is 1.4% in  $H_{max}$  and 2.7% in  $H_s$ . The average  $H_{max}$  during October 2013 from buoy data is 2.92 m and that from ERA5 is 3.34 m indicating an overall positive bias of 0.43 m. But the average  $H_s$  from ERA5 is 1.78 m and the buoy data is 1.91 m indicating a negative bias of 0.13 m. The maximum  $H_{max}$  measured in the North Atlantic Ocean is ~27.3 m between Iceland and the United Kingdom (~59° N, 11° W) by the buoy at 0600 UTC on 4 February 2013 (WMO, 2016) and the corresponding ERA5  $H_{max}$  is 26.4 m, indicating an underestimation of only ~3%.

## Wave period

The annual mean  $T_e$  is underestimated with a negative bias of 0.28 s at Gopalpur, whereas at Ratnagiri it was overestimated with a positive bias of 0.11 s (Table 2). The annual mean  $T_p$  is



underestimated with the bias of 0.78 to 2.61 s at all locations (Table 2). During the TC Phailin, the maximum value of  $T_e$  is 15.5 s, whereas the maximum wave period in ERA5 is 10.7 s (Fig. 2). The average  $T_e$  during October 2013 is 9.4 s from buoy data and is 8.3 s in ERA5 with an overall negative bias of 1.1 s. The average  $T_p$  during October 2013 covering the TC Phailin from buoy data is 12.7 s and that of ERA5 is 10.6 s with an overall negative bias of 2.1 s (Fig. 4).

### 3. Results and discussions

#### 3.1 Spatial and temporal variability of wind and waves in the Indian Ocean

The annual and monthly mean values of wind speed and wave height ( $H_s$  and  $H_{max}$ ) were calculated in the IO (Figs. 5 and 6). The strongest summer mean wind speeds in the southern hemisphere occur in the extra-tropical storm tracks. From April to September, the monthly average wind speed is more than 9 m/s at 61-62° E; 69-70° S and in other months it is more than 8 m/s. The intra-annual variability of the mean wind speeds in the SIO is lower compared to the NIO. A key feature of the monthly mean wind (surface) is the year-round presence of strong easterlies across the 10-30° S region due to the south-easterly trade winds, whereas strong westerlies dominate the south of 40° S (higher extra-tropical latitudes) with least longitudinal changes (Fig. 5). Meridional winds are weak over the SO and here the wind is primarily westerly with a peak monthly mean magnitude of 9 m/s and the temporal patterns in the zonal wind do not change dramatically in the SO (Fig. 5). From June to September, the winds over the AS also reach monthly mean values over 10 m/s. Monthly average wind is strongest (~14.1 m/s) in the central AS region in July. Throughout the year, in the equatorial region, the zonal winds are weak and westerly. Young (1999) and Semedo *et al.* (2011) observed that wind speeds are lowest in the tropical and low latitudes and are highest in the mid- to high-latitudes, along the extra-tropical storm tracks.

Monthly mean wave heights were used to analyze the temporal variability. The NIO is largely seasonal with energetic waves during June-September and relatively calm conditions during the remaining months. In the IO, the  $H_s$  is strongest in the region 48-52° S, 89-93° E, with monthly average values ranging from 3.9 m in December to 5.7 m in July and August (Fig. 6). The monthly mean  $H_{max}$  in the same region ranges from 7.3 to 9.9 m (Fig. 6). In June and July, the monthly mean  $H_s$  along the SO storm belt reaches values up to 7.3 m (Fig. 6), and in April, May, August to October these values are still high, with mean  $H_s$  higher than 5 m. Monthly mean  $H_{max}$  in the SO is highest in September in the region 65-66° S; 50-51° E with values of 14.9 m. Consistent with Anoop *et al.* (2015), the peak magnitude of  $H_s$  over the AS region is in the western region and is in July. The magnitude of  $H_s$  in the AS region is higher than that in the BOB. The wave climate of a major part of

the eastern shelf seas of India is influenced by the Sri Lankan landmass (Anoop *et al.*, 2015). Recently Semedo *et al.* (2018) observed that the waves generated in the SO belt propagate eastward as swell all year round and reach the West Australia coast, also propagate wave energy across the entire IO basin. Zheng and Li (2017) observed that ~30 hr is required for the swell of the Roaring Forties and Furious Fifties (also referred as SO storm belt located between 30° to 60° S) to fully respond to the wind in that region and it takes ~132–138 hr for  $H_s$  to propagate from the Roaring Forties to the NIO. The monthly average  $H_s$  in the SO from 0 to 180° E is examined to know the influence of SO waves in the IO (Fig. 7). The higher monthly mean  $H_s$  in the SO is in the Indian sector of SO and is from June to October. The wave data is not available when ice is formed in the SO and hence the average values presented here are excluding this period for regions south of 55° S.

The energetic wind conditions in the SO create enormous fetch for wave growth, making this region a swell generating area and it propagate throughout the IO. The entire southern region of IO has high wave amplitude compared to the NIO due to the strong Westerlies in 30–60°S and long fetch due to the absence of land masses (Young, 1999). Peak amplitudes of  $H_s$  and  $H_{max}$  in the IO are 16.7 m and 32.0 m and is at 29.5° S, 63° E. Generally the region spanning 41–59° S, 50–74° E has high waves (Fig. 8). The spatial distribution of the maximum value of  $H_s$  and  $H_{max}$  in different months shows that in all months, the maximum value of  $H_s$  and  $H_{max}$  is at locations south of 40° S latitude except in January to March, during which the highest value is at ~19–30° S and is due to the TCs (Table 3). In January, the high  $H_s$  of 15.8 m is at 19° S, 61° E and is generated by intense TC Geralda on 26 January 1993. In February 2007, the high  $H_s$  (~14.4 m) is at 24° S, 52.5° E and is generated due to intense TC Gamede in the western IO off the coast of Madagascar. In the NIO,  $H_s$  more than 8 m occurred in northern BoB in April, May, October and November due to TCs and during the same period  $H_{max}$  more than 14 m occurred (Fig. 8). Similarly in AS, the  $H_s$  more than 8 m is in June. At 50–60° S, only 25% of the time in a year,  $H_{max}$  is less than 5 m indicating the fact that severe wave events are common in this part of the ocean. Hemer *et al.* (2010) reported the focus of wave energy in the region 98–100° E which is located Southwest of Australia and is the most severe wave conditions on the globe. Severe wave climate is reported in the SIO due to the intense mid-latitude cyclones, strongest depressions found outside tropical waters, that traverse the southern waters of the IO (Buckley and Leslie, 2004). The monthly variation of the  $H_s$  indicates a considerable increase of  $H_s$  in June, July and August in the NIO due to the south-westerly monsoon. Also, the mid-latitudes of the SIO show an increase in  $H_s$  during June to September. The southern parts of the SIO experiences high waves all year-round while it is lower from November to March.

The superposition of low-frequency swell waves with high-frequency wind-waves is one of the cause for freak-waves. Other potential causes are the effects of currents, modulation instability etc. One of the criteria of defining freak-waves is  $H_{\max}/H_s > 2$ . At most of the locations  $H_{\max}/H_s$  exceeded 2 at least once, indicating there are potential freak-wave cases during 1979 to 2017 (Fig. 9). The  $H_{\max}/H_s$  ratio in the study area varies from 1.46 to 2.3 with an average value of 1.87 during 1979-2017. Amrutha and Kumar (2017) observed that in the coastal waters of the eastern Arabian Sea, the  $H_{\max}/H_s$  ratio is 1.50 to 1.62 times the  $H_s$  for different locations.

In the earlier sections, monthly average, yearly average and annual maximum wave characteristics are discussed. In order to know the temporal variation of hourly  $H_s$  and  $T_p$  over a year along longitude, the time series data at 5 locations ( $20^\circ$  N,  $0^\circ$ ,  $20^\circ$  S,  $40^\circ$  S,  $60^\circ$  S) along  $65^\circ$  E and 5 points along  $90^\circ$  E for the year 2017 is examined (Fig. 10). In the AS ( $20^\circ$  N,  $65^\circ$  E), the intra-annual variability of  $H_s$  shows a gradual increase from May to July and then a decrease from July to December, whereas such large seasonal variations are not observed at other locations. At  $40^\circ$  and  $60^\circ$  S, the annual mean  $H_s$  is 3.5 to 3.6 m, whereas the annual maximum value is 12 m. At  $20^\circ$  S, the wave activity reduces and the annual average  $H_s$  is 2.7 m with an annual maximum of  $\sim 5$  m. From  $40^\circ$  to  $20^\circ$  S ( $\sim 2222$  km), the waves lose around 75% of the energy. Ardhuin *et al.* (2009) reported that steep swell loses a significant fraction ( $\sim 65\%$ ) of its energy over a distance of  $\sim 2800$  km. Among the 5 locations, the equator has the least wave intensity with annual average  $H_s$  of 1.5 and annual maximum value of 2.6 m along the  $65^\circ$  longitude. While at  $90^\circ$  E, the annual maximum is 4 m and the average value is 2 m. In the NIO, the annual maximum value is 4.7 m with an average value of 1.4 m in BoB, whereas in AS, it is 4.2 m and 1.6 m respectively (Fig. 10).

Characterizing the wave climate in a region by using the  $H_s$  and mean wave period might not be enough since the wave climate contains two or more different wave fields generated at different locations. Hence, the wind-sea and swell heights are examined separately. The monthly average wind-sea and swell heights are maximum from July to September both in the SIO and NIO (Fig. 11). Similar to  $H_s$  and  $H_{\max}$ , the maximum value of wind-sea and swell  $H_s$ , also are at locations south of  $40^\circ$  S latitude except those during the TCs. In January, the highest wind-sea  $H_s$  of 15.8 m is at  $19^\circ$  S,  $61^\circ$  E and is generated by intense TC Geralda on 26 January 1993 (Table 3). The monthly average swell wave heights are higher than the monthly average wind-sea ones in most of the months (Fig. 11). The ratio of the wind-sea and the swell heights are presented in logarithmic scale and hence the positive contours indicate locations with wind-sea heights more than the swell heights and the negative contours indicate vice-versa. The spatial pattern of the ratio of the wind-sea and swell wave

heights reveals that the entire IO is swell dominated during most of the time (Fig. 12). Despite the strong Asian monsoon generating local wind-sea waves in summer in the AS and BoB, waves keep being generated along the SO storm belt in the IO. Swells propagate northward as swells and reach the NIO. The maximum wind speed ranged from 30 m/s in October to 35.1 m/s in February (Table 4). Except in the offshore of Somalia and the region between Indian and Sri Lanka (Gulf of Mannar and Palk Bay), the monthly mean swell wave heights are clearly higher than the locally generated wave heights. When wind-sea and swell wave heights are compared, mostly along the offshore of Somalia from June to September and from December to February, wind-sea  $H_s$  is more than the swell  $H_s$  because of the strong cross-equatorial winds of the Somali (Findlater) jet (Findlater, 1969). Even though swell  $H_s$  is more than the wind-sea  $H_s$ , in the SO, the wind-sea  $H_s$  is comparable to swell  $H_s$  indicating this region as a wave generation area. Similarly from December to February, north-eastern AS also have comparable wind-seas. Except for the period from November to February, the equatorial region has swells with negligible wind-seas (Fig. 12). Semedo *et al.* (2011) shown that more than 75% of the time, the global wave field is dominated by swells. When the maximum value of the wind-sea and swell heights are considered, the wind-sea heights are maximum with values from 13.4 to 15.9 m compared to the swell heights (9 to 12.4 m) (Table 3). In the SO also during most of the period, swell domination is noted and comparable wind-sea heights are observed from July to October (Fig. 12).

The monthly average value of the mean wave period at most areas ranges from 7 to 13 s except in the northern AS, where lower wave periods are observed from November to February (Fig. 13). The maximum value of the mean wave period varied from 15.9 to 17.2 s in different months (Table 4). The storms in the SO generate the highest and longest waves in the IO with typical monthly mean wave periods between 10 and 12 s during May to September (Fig. 13). Hemer *et al.* (2010) observed that longest wave periods are in a zonal band at approximately 30° S due to the arrival of the SO storms generated waves. The mean wave period decreases to the north of 30° S as the swell energy dissipates with distance from SO storms and locally generated sea waves begin to dominate (Hemer *et al.*, 2010). The lowest mean wave period is in the northern AS during November to February due to the low waves and low wind. The peak wave periods are large (> 13 s) at the region around 30° S, ranging from 70° to 100° E. The maximum value of the peak wave period is 24 s.

### 3.2 Trends in wave parameters during 1979-2017

Long-term changes in waves are characterized by trends in annual mean  $H_s$ ,  $H_{max}$  and annual maximum  $H_s$  and  $H_{max}$  during 1979-2017. Annual mean trends for 4 seasons as per World Meteorological Society standards: i) Summer (Winter) from December to February, ii) Autumn (Spring) from March to May, iii) Winter (Summer) from June to August and iv) Spring (Autumn) from September to November in southern (northern) hemisphere are also presented in Figure 14. In the IO, the annual mean  $H_s$  increased by 0.3 to 0.6 m/year in different seasons with relatively maximum during March to May. During 1979-2017, overall a positive trend of 0.4 cm/year in annual mean  $H_s$  is observed in the study area and during the same period wind speed also show a positive trend of 2.2 cm/s/year (Fig. 15). In SO, maximum decreasing trend of 1.9 cm/year is observed in annual mean  $H_s$  at 64.75° S; 95° E, whereas maximum increasing trend of 1.7 cm/year is observed at 66.25° S; 49.5° E. Significant positive trends are in the SO during June to September between 2000 and 2017 and are typically greater (~2 cm/year) for annual mean  $H_s$  between 70° and 100° E. In SIO, the maximum decreasing trend of 0.14 cm/year is observed in annual mean  $H_s$  at 43° S; 90.5° E and the maximum increasing trend of 0.9 cm/year is observed at 52.5° S; 73° E (Fig. 14). During 2000-2017, for annual mean  $H_{max}$ , the trend varied from -2 cm/year at 43° S; 90.5° E to 2 cm/year at 58° S; 86° E. The annual maximum  $H_s$  showed larger trends compared to the annual mean  $H_s$  with values ranging from -11 to 9 cm/year during 1979-2017 and -17 to 19 cm/year during 2000-2017, whereas the annual maximum  $H_{max}$  showed much higher trends ranging from -21 to 18 cm/year with average value of 0.97 cm/year for the study area during 1979-2017 (Fig. 15). The annual mean  $H_{max}$  showed trends ranging from -6 to 4 cm/year with an average value of 0.73 cm/year for the study area. Hemer *et al.* (2010) reported significant positive trends (~5 cm/year) between 1991 and 2006 in altimeter-measured  $H_s$  in the Pacific and Indian sectors of the SO during July and September and the increasing trend is due to the southward shift of the SO storm belt, generating larger wave heights resulting from stronger westerly winds in the southern latitudes. Zheng and Li (2017) using the ERA-40 data from 1957 to 2002, reported that the  $H_s$  show significant increasing trends of 0.30-0.68 cm/year. The SIO winds are stronger than that those over the NIO and the winds of the SIO show a significant increasing trend of 0.34–1.31 cm/s/year during 1957 to 2002 (Zheng and Li, 2017). The principal mode of inter-annual variability of the waves in Southern Hemisphere is related to the Southern Annular Mode by Hemer *et al.* (2010).

With the advent of long marine Earth-observing satellite missions (European Remote Sensing Satellites ERS-1 and ERS-2, starting in 1991), the quality and coverage of marine wind speed and  $H_s$

observations rose dramatically (Aarnes *et al.*, 2015). Since such observations are usually assimilated into global reanalyses, the quality of a reanalysis before and after the satellite era are different and hence trends in the analysis will be spuriously affected if we combine data before and after 1992 (Aarnes *et al.*, 2015). Hence, the trend presented in this article from 1979 to 2017 is to be looked with caution and in order to show the difference in trend during 1979 to 1990 and from 1991 to 2017, the trend of annual mean  $H_s$  and annual maximum  $H_s$  during both periods are presented in Fig. 15. The average trend in annual mean  $H_s$  during 1991 to 2017 in the study area is -0.07 cm/year and that in annual maximum  $H_s$  is -0.64 cm/year. Further, 5 locations along  $70^\circ$  E is selected along with two coastal stations in AS and BoB and the trend of annual average  $H_s$  in different periods is presented in Fig. 16. Positive trends varying from 0.11 to 0.87 cm/year (Table 5) are observed at these locations during 1979-2017, whereas at the same locations except at  $60^\circ$  S;  $70^\circ$  E, negative trend varying from 0.13 to 0.48 cm/year are observed from 1991 to 2017 indicating that the reanalysis data has to be used with caution for long-term trend analysis since the quantity and quality of the data being assimilated changes in time especially before and after the satellite era. In fact, trends themselves can change over time and the result above might be the reflection of their interannual variability rather than issues with reanalysis datasets. At  $60^\circ$  S;  $70^\circ$  E, positive trend of 0.08 cm/year is observed from 1991 to 2017, which is 0.03% compared to the earlier projection of 6-9% increase in IO (Mori *et al.*, 2010). The trend based on ERA-Interim data (0.01 to 0.3 cm/year) is much less than that based on ERA5 data except for the southernmost point (Fig. 16). At most of the locations the trend presented are statistically significant at more than 90% from the Mann Kendall Test (Table 5).

### 3.3 Long-term statistical analysis of wave height

Estimates of the values of  $H_s$  likely to be encountered (extreme waves) is required for the design of vessels and ocean structures. Extreme waves are estimated for all the locations to study the spatial distribution of wave height with 50 and 100-year return periods using the 39-year ERA5 dataset following the long-term statistical analysis of waves based on GEV distribution using annual maxima  $H_s$  and that based on GPD using POT (Fig. 17). There are slight changes in the return level estimate using GEV and GPD. The maximum value of 17.8 m for 100-year return levels with GEV is at  $58.5^\circ$  S;  $72.5^\circ$  E (Fig. 17). At the same location, the 50-year return level with GEV is 16.4 m, whereas GPD estimate gives 17.5 m and 16.3 m as 100 and 50-year return levels. The largest ever recorded wave height in the SO up to 2017 is 22 m (recorded in 2012) by the Australian buoy (<http://www.metocean.co.nz/news>). Recently on 8 May 2018, a wave buoy moored in the Southern Ocean by MetOcean Solutions recorded a  $H_{max}$  of 23.8-m with  $H_s$  of 14.9 m. In the coastal waters of

AS, the 100-year return levels are relatively low ( $< 8$  m), whereas values up to 12 m are present in some stretches of coastal waters of north-western BoB.

The variations in wave height with 39, 50 and 100-year return level with data duration varying from 10, 15, 20, 25, 30 and 35 years with 39 years is presented in Fig. 18. It is observed that the difference in 100-year return level of  $H_s$  for 10-year and 39-year data block varies from -6 to 7 m. The changes are larger in the region 23 to 26° S and in small areas in AS and BoB (Fig. 18). The difference in the return level of  $H_s$  is due to the high values occurred in a particular year. For e.g., at 63.5° E; 20.5° S, highest  $H_s$  of 13.7 m is in 2003, whereas the maximum  $H_s$  from 2010 to 2018 is 8.7 m. Hence, adding small values in the data sets at this location resulted in lowering the 100-year return level by 6 m. Similarly at 74° E; 24° S, the maximum  $H_s$  is in 2015 (11 m) and 2016 (10.5 m), whereas in other years up to 2009, the maximum value is 6.2 m. Hence, adding two high values resulted in an increase of 3 m in the 100-year return level. The 100-year return level based on 39-year data at 25.5° S, 79° E is 13.3 m, whereas that based on recent 10-year data is 21.7 m since very high waves are generated in this area by TCs in recent years ( $H_s$  of 12.8 m in December 2013, 10.2 m in January 2015, 8.8 m in February 2007 and 8.2 m in 2016). It has to be noted that a single large wave can influence the return levels in annual maxima by GEV distribution. Even though ten years is the minimum period of data required to estimate the 100-year return value (Goda, 2010), the occurrence of occasional very high values alter the  $H_s$  with different return periods. Agarwal *et al.* (2013) observed that when the period of data was increased beyond 15 years, the change in 100-year return value is negligible. Whereas, in the present study, the change in the 100-year return value for data periods beyond 15 years is up to 6 m. From the general perspective, if the climate is characterized by at least 30-years time series, it may reflect that 30 years is more or less enough for a reasonable representation of mean state and it should be the lowest bound for estimating the return periods.

#### 4. Conclusions

In this study, we examined the ERA5 wave parameters (significant wave height, maximum wave height, mean wave period and peak wave period) and wind speed over the IO and SO region during 1979-2017. Annual mean wave heights were determined by averaging the 1-hourly data and are used for describing the characteristics of the annual cycle, its variability and the climatological trends. Monthly mean  $H_s$  is largest in the IO in July and is shortest in December. In all months, the maximum value of  $H_s$  and  $H_{max}$  occur south of 40° S except in January, February and December, during which the maximum values are at ~19-25° S and are due to the TCs. The SIO wave height

seasonality is lower than that in the NIO. In the IO, except in the offshore of Somalia and the region between India and Sri Lanka (Gulf of Mannar and Palk Bay), the monthly mean swell wave heights are higher than the locally generated wave heights in all the months. During 1979-2017, the average trend of annual mean  $H_s$  in the study area is 0.4 cm/year and it changes to -0.07 cm/year when data from 1991 to 2017 are used. Extreme caution should be taken when reanalysis data is used for trend reanalysis since the quantity and quality of the data being assimilated changes in time. When the period of data was decreased from 39 to 20 years, the 100-year return level of  $H_s$  changed by -4 to 5 m.

### **Acknowledgments**

This research would not have been possible without the availability of the ERA5 data provided by the ECMWF. ERA5 data used in this study have been obtained from the ECMWF data server: <http://data.ecmwf.int/data>. The authors acknowledge ESSO-Indian National Centre for Ocean Information Services (INCOIS), Ministry of Earth Sciences, Government of India for funding the wave measurement program and Council of Scientific and Industrial Research, New Delhi for funding the research work. We thank Dr. T.M. Balakrishnan Nair, Head, OSISG and Mr. Arun Nherakkol, Scientist, INCOIS, Hyderabad and Mr. Jai Singh, Technical Assistant, CSIR-NIO for help during the coastal data collection. The authors thank Centre for Coastal & Marine Biodiversity, Dr. Babasaheb Ambedkar Marathwada University, Ratnagiri and Chilka Development Authority, Odisha for providing the logistics required for wave data collection. We thank the two reviewers and the Editor for the suggestions which improved the scientific content of this paper. This work is a part of the Doctoral thesis of the first author registered with Bharathidasan University, Tiruchirappalli. This publication is a NIO contribution -----.



## References

- Aarnes, O.J., Abdalla, S., Bidlot, J. R. and Breivik, Ø. (2015) Marine wind and wave height trends at different ERA-Interim forecast ranges. *Journal of Climate*, 28(2), 819-37.
- Agarwal, A., Venugopal, V. and Harrison, G.P. (2013) The assessment of extreme wave analysis methods applied to potential marine energy sites using numerical model data. *Renewable and Sustainable Energy Reviews*, 27, 244–257.
- Amrutha, M.M. and Sanil Kumar, V. (2017) Characteristics of high monsoon wind-waves observed at multiple stations in the eastern Arabian Sea, *Ocean Science Discussions*, <https://doi.org/10.5194/os-2017-84>.
- Amrutha, M.M., Sanil Kumar, V. and Jesbin George (2017) Observations of long-period waves in the nearshore waters of central west coast of India during the fall inter-monsoon period, *Ocean Engineering*, 131, 244-262, 10.1016/j.oceaneng.2017.01.014.
- Amrutha, M.M., Sanil Kumar, V., Sandhya, K.G., Balakrishnan Nair, T.M. and Rathod, J.L. (2016) Wave hindcast studies using SWAN nested in WAVEWATCH III - comparison with measured nearshore buoy data off Karwar, eastern Arabian Sea, *Ocean Engineering* 119C, 114-124. 10.1016/j.oceaneng.2016.04.032.
- Amrutha, M.M., Sanil Kumar, V., Anoop, T.R., Balakrishnan Nair, T.M., Arun Nherakkol, and Jeyakumar, C. (2014) Waves off Gopalpur, northern Bay of Bengal during the Cyclone Phailin, *Annales Geophysicae*, 32, 1073-1083, doi:10.5194/angeo-32-1073-2014.
- Anjali Nair, M. and Sanil Kumar, V. (2016) Spectral wave climatology off Ratnagiri - northeast Arabian Sea, *Natural Hazards*, 82, 1565-1588. 10.1007/s11069-016-2257-5.
- Anjali Nair, M. and Sanil Kumar, V. (2017) Wave spectral shapes in the coastal waters based on measured data off Karwar on the west coast of India, *Ocean Science*, 13, 365–378, doi:10.5194/os-13-365-2017.
- Anjali Nair, M., Sanil Kumar, V., Amrutha, M.M. and Murty, V.S.N. (2019) Features of locally and remotely generated surface gravity waves in the inner-shelf region of north-western Bay of Bengal, *International Journal of Climatology*, 39:1644-1664 doi: 10.1002/joc.5907.
- Anoop, T.R., Kumar, V.S., Shanas, P.R. and Glejin, J. (2015) Surface wave climatology and its variability in the North Indian Ocean based on ERA-Interim reanalysis, *J. Atmos. Oceanic Technol.* 32(7), 1372-1385. doi.: 10.1175/JTECH-D-14-00212.1.
- Anoop, T.R., Sanil Kumar, V. and Shanas, P.R. (2014) Spatial and temporal variation of surface waves in shallow waters along eastern Arabian Sea. *Ocean Engineering*, 81, 150-157, doi: 10.1016/j.oceaneng.2014.02.010.
- Ardhuin, F., Chapron, B. and Collard, F. (2009) Observation of swell dissipation across oceans, *Geophysical Research Letters*, 36, L06607, <http://dx.doi.org/10.1029/2008gl037030>.
- Bertin, X., Prouteau, E. and Letetrel, C. (2013) A significant increase in wave height in the North Atlantic Ocean over the 20th century, *Glob. Planet. Change*, 106, 77–83, <https://doi.org/10.1016/j.gloplacha.2013.03.009>.

- Buckley, B. W. and Leslie, L. M. (2004) Preliminary climatology and improved modelling of south Indian Ocean and Southern Ocean mid-latitude cyclones. *Int. J. Climatol.*, 24: 1211-1230. doi:10.1002/joc.1050.
- Burkey, J. (2006) A non-parametric monotonic trend test computing Mann-Kendall Tau, Tau-b, 447 and Sen's Slope written in Mathworks-MATLAB implemented using matrix rotations, King 448 County, Department of Natural Resources and Parks, Science and Technical Services section, 449 Seattle, Washington, USA.
- Caires, S. and Sterl, A. (2005) 100-Year return value estimates for ocean wind speed and significant wave height from the ERA-40 data. *Journal of Climate*. 18, 1032-1048. doi: 10.1175/JCLI-3312.1.
- Castelle, B., Dodet, G., Masselink, G., and Scott, T. (2018) Increased winter-mean wave height, variability, and periodicity in the northeast Atlantic over 1949–2017. *Geophysical Research Letters*, 45, 3586–3596. <https://doi.org/10.1002/2017GL076884>.
- Cavaleri, L. and Sclavo, M. (2006) The calibration of wind and wave model data in the Mediterranean Sea. *Coastal Engineering*, 53,613–627.
- Coles, S., Bawa, J., Trenner, L., and Dorazio, P. (2001) An introduction to statistical modeling of extreme values, *Springer-Verlag*, London., UK., 205pp.
- Cooper, C.K. and Forristall, G.Z. (1997) The Use of Satellite Altimeter Data to Estimate the Extreme Wave Climate. *J. Atmos. Oceanic Technol.*, 14, 254–266.
- Cox, A.T. and Swail, V.R. (2001) A global wave hindcast over the period 1958-1997. *J. Geophysical Research Ocean* 106:2313–29.
- Datawell (2009) Datawell Waverider Reference Manual, *Datawell BV oceanographic instruments*, The Netherlands, pp 123.
- Dee, D. P., Uppala, S. M., Simmons, A.J., Berrisford, P., Poli, P., Kobayashi, S., Andrae, U., Balmaseda, M.A., Balsamo, G., Bauer, P., Bechtold, P., Beljaars, A.C.M., van de Berg, L., Bidlot, J., Bormann, N., Delsol, C., Dragani, R., Fuentes, M., Geer, A.J., Haimberger, L., Healy, S.B., Hersbach, H., Hólm, E.V., Isaksen, L., Kållberg, P., Köhler, M., Matricardi, M., McNally, A.P., Monge-Sanz, B.M., Morcrette, J.J., Park, B.K., Peubey, C., de Rosnay, P., Tavolato, C., Thépaut, J.N. and Vitart, F. (2011) The ERA-Interim reanalysis: Configuration and performance of the data assimilation system, *Q. J. Roy. Meteor. Soc.*, 137, 553–597.
- Fan, Y., Held, I.M., Lin, S. and Wang, X.L. (2013) Ocean Warming Effect on Surface Gravity Wave Climate Change for the End of the Twenty-First Century. *J. Climate*, 26,6046–6066.
- Findlater, J. (1969) A major low-level air current near the Indian Ocean during the northern summer. *Quart. J. Roy. Meteor. Soc.* 95(404), 362-380. doi:10.1002/qj.49709540409.
- Glejin, J., Kumar, V.S., Anoop, T.R. and Joseph, J. (2016) Directional characteristics of shallow water waves along south western Bay of Bengal, *Ocean Engineering* 121, 546-558. 10.1016/j.oceaneng.2016.06.006
- Goda, Y. (1992) Uncertainty of design parameters from viewpoint of extreme statistics, *J Offshore Mech Arct.*, 114(2), 76-82, 1992.

Goda, Y. (2010) Random Seas and Design of Maritime Structures. *World Scientific Publishing Co Pte Ltd*, 3rd edition. ISBN 9789814282406.

Gulev, S.K., Grigorieva, V., Sterl, A. and Woolf, D. (2003) Assessment of the reliability of wave observations from voluntary observing ships: insights from the validation of a global wind wave climatology based on voluntary observing ship data. *J. Geophys. Res. Oceans* 108(C7): 3236. <https://doi.org/10.1029/2002JC001437>.

Hemer, M.A., Church, J.A. and Hunter, JR. (2010) Variability and trends in the directional wave climate of the Southern Hemisphere. *International Journal of Climatology*, 30: 475–491. <https://doi.org/10.1002/joc.1900>.

Hersbach, H. and Dee, D. (2016) ERA5 reanalysis is in production. *ECMWF Newsletter* 147.7.

Hithin, N.K., Kumar, V.S. and Shanas, P.R. (2015) Trends of wave height and period in the Central Arabian Sea from 1996 to 2012: A study based on satellite altimeter data. *Ocean Engineering*, 108, 416-425. doi: 10.1016/j.oceaneng.2015.08.024.

Izaguirre, C., Mendez, F., Menendez, M. and Losada, I.J. (2011) Global extreme wave height variability based on satellite data. *Geophysical Research Letters*, 38: L10607. <https://doi.org/10.1029/2011GL047302>.

Kumar, D., Sannasiraj, S.A., Sundar, V. and Polnikov, V.G. (2013) Wind-Wave Characteristics and Climate Variability in the Indian Ocean Region Using Altimeter Data. *Marine Geodesy*. 36(3), 303-318.

Kundzewicz, Z.W. and Robson, A. (2000) Detecting Trend and Other Changes in Hydrological Data World Climate Programme Data and Monitoring. WMO/TD-No. 1013, Geneva.

Lecacheux, S., R., Pedreros, G., Le Cozannet, J., Thiébot, Y., De La Torre and Bulteau, T. (2012) A method to characterize the different extreme waves for islands exposed to various wave regimes: a case study devoted to Reunion Island. *Nat. Hazards Earth Syst. Sci.*, 12, 2425-2437.

Liang, B., Gao, H. and Shao, Z. (2019) Characteristics of global waves based on the third-generation wave model SWAN, *Marine Structures*, 64, 35-53.

Martucci, G., Carniel, S., Chiggiato, J., Sclavo, M., Lionello, P. and Galati, M. B. (2010) Statistical trend analysis and extreme distribution of significant wave height from 1958 to 1999 – an application to the Italian Seas, *Ocean Science*, 6, 525–538.

Mori, N., Yasuda, T., Mase, H., Tom, T. and Oku, Y. (2010) Projection of extreme wave climate change under global warming. *Hydrol. Res. Lett.*, 4, 15–19.

Naseef, T.M., Sanil Kumar, V. (2017) Variations in return value estimate of ocean surface waves – a study based on measured buoy data and ERA-Interim reanalysis data, *Natural Hazards Earth System Sciences*, 17, 1763–1778, doi: 10.5194/nhess-17-1763-2017.

Patra, S.K., Mishra, P., Mohanty, P.K., Pradhan, U.K., Panda, U.S., Murthy, M.V.R., Kumar, S.K and Nair, T.M.B. (2016) Cyclone and monsoonal wave characteristics of northwestern Bay of Bengal: long-term observations and modeling, *Natural Hazards*, 82, 1051–1073. doi 10.1007/s11069-016-2233-0.

- Premkumar, K., Ravichandran, M., Kalsi, S.R., Sengupta, D. and Gadgil, S. (2000) First results from a new observational system over the Indian Seas. *Current Science India*. 78(3), 323-330.
- Reguero, B.G., Losada, I.J. and Méndez, F.J. (2019) A recent increase in global wave power as a consequence of oceanic warming. *Nature Communications* 10 (1), doi: 10.1038/s41467-018-08066-0.
- Sandhya, K.G., Balakrishnan Nair, T.M., Bhaskaran, P.K., Sabique, L., Arun, N. and Jeykumar, K. (2014) Wave forecasting system for operational use and its validation at coastal Puducherry, east coast of India. *Ocean Engineering*, 80, 64-72.
- Sanil Kumar, V. and Muhammed Naseef T. (2015) Performance of ERA-Interim wave data in the nearshore waters around India. *Journal of Atmospheric and Oceanic Technology*, 32, 6, 1257-1269. doi.:10.1175/JTECH-D-14-00153.1.
- Sanil Kumar, V., Dubhashi, K.K. and Balakrishnan Nair, T.M. (2014) Spectral wave characteristics off Gangavaram, Bay of Bengal, *Journal of Oceanography*, 70:307–321,doi 10.1007/s10872-014-0223-y.
- Sanil Kumar, V., Jossia Joseph, Amrutha, M.M., Jena, B.K., Sivakholundu, K.M. and Dubhashi, K.K. (2018) Seasonal and interannual changes of significant wave height in shelf seas around India during 1998 to 2012 based on wave hindcast, *Ocean Engineering*, 151, 127–140, doi.org/10.1016/j.oceaneng.2018.01.022.
- Schott, F. and McCreary, J.P. (2001) The Monsoon Circulation of the Indian Ocean. *Progress Oceanography*, 51, 1-123, [https://doi.org/10.1016/S0079-6611\(01\)00083-0](https://doi.org/10.1016/S0079-6611(01)00083-0).
- Semedo, A., Soares, P.M.M. and Lemos, G. (2018) Waves along Eastern boundary currents – The regional winds effect, *Ocean Modelling*, 129, 39-57, doi.org/10.1016/j.ocemod.2018.07.005.
- Semedo, A., Sušelj, K., Rutgersson, A. and Sterl, A. (2011) A global view on the wind sea and swell climate and variability from ERA-40. *Journal of Climate*, 24:1461–1479, doi: 10.1175/2010JCLI3718.1.
- Sen, P.K. (1968) Estimates of the Regression Coefficient Based on Kendall's Tau, *J. American Statistical Association*, 63, 1379-1389, DOI: 10.1080/01621459.1968.10480934
- Shanas, P.R. and Sanil Kumar, V. (2015) Trends in surface wind speed and significant wave height as revealed by ERA-Interim wind wave hindcast in the Central Bay of Bengal, *International Journal of Climatology*, 35, 2654–2663. doi: 10.1002/joc.4164.
- Sterl, A., Komen, G. J., and Cotton, P. D. (1998) Fifteen years of global wave hindcasts using winds from the European Centre for Medium-Range Weather Forecasts reanalysis: Validating the reanalyzed winds and assessing the wave climate, *J. Geophys. Res.*, 103( C3), 5477– 5492, doi:10.1029/97JC03431.
- Stopa, J.E. and Cheung, K.F. (2014) Intercomparison of Wind and Wave Data from the ECMWF Reanalysis Interim and the NCEP Climate Forecast System Reanalysis. *Ocean Modelling*, 75, 65-83.
- Tucker, M.J. and Pitt, E.G. (2001) Waves in ocean engineering, *Elsevier, Amsterdam*. p548.

- Vinoth, J. and Young, I. R. (2011) Global estimates of extreme wind speed and wave height. *Journal of Climate*, 24, 1647-1665. doi: 10.1175/2010JCLI3680.1.
- Wang, X.L., Feng, Y. and Swail, V. R. (2014) Changes in global ocean wave heights as projected using multimodel CMIP5 simulations. *Geophysical Research Letters*, 41, 1026-1034, doi:10.1002/2013GL058650.
- WMO (2016) 19-meter wave sets new record - highest significant wave height measured by a buoy, Press release, <https://public.wmo.int/en/media/press-release/19-meter-wave-sets-new-record-highest-significant-wave-height-measured-buoy> (accessed on 13 April 2019).
- Young, I. R., Zieger, S. and Babanin, A. V. (2011) Global trends in wind speed and wave height, *Science*, 332(6028), 451-455. <https://doi.org/10.1126/science.1197219>.
- Young, I.R. (1999) Seasonal variability of the global ocean wind and wave climate. *International Journal of Climatology*, 19: 931–950.
- Young, I.R. and Ribal, A. (2019) Multiplatform evaluation of global trends in wind speed and wave height. *Science*, 2019; eaav9527 doi: 10.1126/science.aav9527.
- Zheng, C.W. and Li, C.Y. (2017) Analysis of temporal and spatial characteristics of waves in the Indian Ocean based on ERA-40 wave reanalysis, *Applied Ocean Research*, 63, 217–228.

Table 1. Measurement locations and the water depth

Location	Buoy		ERA5		Period of validation
	Latitude Longitude	Water depth (m)	Latitude Longitude	Water depth (m)	
off Ratnagiri, eastern Arabian Sea	16.980° N; 73.258° E	13	17.10° N; 73.20° E	47	1 January 2015 to 31 December 2015
off Gopalpur, western Bay of Bengal	19.282° N; 84.964° E	15	19.20° N; 85.20° E	97	1 January 2015 to 31 December 2015  1 October 2013 to 15 October 2013
Central Arabian Sea	15.00° N; 69.01° E	3000	15.00° N; 69.00° E	3000	1 February 2012 to 31 December 2012
Central Bay of Bengal	12.15° N; 90.75° E	2700	12.00° N; 90.50° E	2700	1 January 2003 to 31 December 2003

Table 2. Comparison statistics of buoy data and ERA5 data in coastal waters for significant wave height, maximum wave height, mean wave period and peak wave period

	Ratnagiri	Goplapur during TC	Gopalpur
Number of data	8756	162	8759
Significant wave height (m)			
Buoy mean	1.06	2.56	1.00
ERA5 mean	1.03	2.46	1.03
R	0.98	0.98	0.94
RMSE (m)	0.15	0.36	0.15
Bias (m)	-0.04	-0.10	0.03
Maximum wave height (m)			
Buoy mean	1.63	3.93	1.52
ERA5 mean	1.92	4.62	1.95
R	0.97	0.96	0.91
RMSE (m)	0.40	1.15	0.52
Bias (m)	0.29	0.69	0.43
Mean wave period (s)			
Buoy mean	7.61	10.77	8.92
ERA5 mean	7.72	9.20	7.92
R	0.83	0.69	0.74
RMSE (s)	0.94	2.30	1.65
Bias (s)	0.11	-1.58	-1.00
Peak wave period (s)			
Buoy mean	11.06	13.45	12.19
ERA5 mean	10.28	11.78	10.00
R	0.63	0.60	0.39
RMSE (s)	3.10	3.58	4.01
Bias (s)	-0.78	-1.67	-2.19

Table 3. Maximum value of significant wave height, maximum wave height, wind-sea  $H_s$  and swell  $H_s$  in different months along with the location of occurrence

Month	$H_s$ (m)		$H_{max}$ (m)		Wind-sea $H_s$ (m)		Swell $H_s$ (m)	
	Value	Location	Value	Location	Value	Location	Value	Location
JAN	15.8	19.5°S; 61.0°E	30.6	19.5°S; 61.0°E	15.8	19.5°S; 61.0°E	11.6	31.0°S; 58.5°E
FEB	14.4	24.0°S; 52.5°E	27.5	24.0°S; 52.5°E	13.9	60.5°S; 20.5°E	10.5	38.5°S; 75.0°E
MAR	16.7	29.5°S; 63.0°E	32.0	29.5°S; 63.0°E	16.6	29.5°S; 63.0°E	12.4	27.5°S; 61.5°E
APR	14.4	56.0°S; 81.0°E	27.4	56.0°S; 81.0°E	13.4	36.5°S; 101.0°E	9.8	58.0°S; 79.5°E
MAY	15.9	65.0°S; 46.0°E	30.5	65.0°S; 47.5°E	15.2	65.0°S; 47.5°E	11.2	64.0°S; 43.5°E
JUN	15.7	59.5°S; 20.0°E	29.2	47.5°S; 44.0°E	15.3	47.5°S; 44.0°E	11.1	60.0°S; 23.0°E
JUL	15.8	46.0°S; 85.5°E	30.1	46.0°S; 85.5°E	15.8	46.0°S; 85.5°E	10.9	53.0°S; 96.0°E
AUG	16.0	51.0°S; 56.0°E	30.6	51.0°S; 56.0°E	15.9	51.0°S; 56.0°E	11.1	57.0°S; 33.0°E
SEP	15.7	52.0°S; 57.5°E	29.5	52.0°S; 57.5°E	15.7	52.0°S; 57.5°E	10.0	57.5°S; 109.5°E
OCT	15.6	59.0°S; 73.5°E	29.3	59.0°S; 73.5°E	14.2	57.0°S; 107.0°E	10.3	56.5°S; 109.5°E
NOV	14.8	51.5°S; 108.0°E	28.1	51.5°S; 107.0°E	14.8	51.5°S; 108.0°E	9.0	56.5°S; 20.5°E
DEC	14.5	53.5°S; 111.0°E	27.4	53.5°S; 111.0°E	14.5	53.5°S; 111.0°E	9.7	56.5°S; 73.0°E



Table 4. Maximum value of wind speed, mean wave period and peak wave period in different months along with the location of occurrence

Month	Wind speed (m/s)		Mean wave period (s)		Peak wave period (s)	
	Value	Location	Value	Location	Value	Location
JAN	44.2	18.25°S; 60.75°E	16.2	34.5°S; 87.0°E	23.7	63.75°S; 28.25°E
FEB	42.5	18.50°S; 53.00°E	15.9	23.0°N; 65.5°E	21.6	69.75°S; 24.50°E
MAR	38.2	19.25°S; 84.75°E	16.2	60.5°S; 113.0°E	21.8	16.00°N; 95.50°E
APR	39.7	21.50°N; 91.50°E	16.7	21.0°S; 55.0°E	21.9	08.50°N; 98.00°E
MAY	38.2	19.50°N; 91.50°E	16.4	22.0°S; 43.0°E	22.2	13.50°N; 93.25°E
JUN	40.5	43.00°S; 65.00°E	16.6	26.0°S; 113.0°E	21.5	26.00°S; 113.00°E
JUL	39.1	51.00°S; 34.75°E	17.5	24.0°S; 113.5°E	21.9	16.50°N; 92.50°E
AUG	39.4	64.50°S; 109.25°E	16.4	60.25°S; 73.0°E	21.6	12.50°N; 86.25°E
SEP	37.5	47.50°S; 88.75°E	16.1	34.0°S; 92.0°E	24.0	37.75°S; 76.75°E
OCT	38.7	46.50°S; 97.25°E	17.2	22.5°S; 112.0°E	21.8	10.25°N; 98.00°E
NOV	37.7	43.25°S; 84.25°E	17.2	18.75°N; 94.5°E	22.0	10.25°N; 98.00°E
DEC	36.8	44.25°S; 73.75°E	16.8	25.25°N; 66.5°E	21.5	08.50°N; 98.00°E

Table 5. Parameters of statistical significance of the trend estimate at selected locations

DATA	Location	Trend		
		P value	(cm/year)	Significance
ERA5 from 1979 to 2017	Honnavar	0.0352	0.11	0.95
	Gopalpur	0.1499	0.12	0.85
	20° N 70° E	0.0926	0.14	0.90
	0° N 70° E	0.0022	0.35	0.95
	20° S 70° E	0.0096	0.37	0.95
	40° S 70° E	0.0500	0.42	0.95
	60° S 70° E	0.0058	0.87	0.95
ERA5 from 1979 to 1990	Honnavar	0.3359	0.28	0.66
	Gopalpur	0.6312	0.28	0.36
	20° N 70° E	0.4507	0.35	0.54
	0° N 70° E	0.0641	0.64	0.93
	20° S 70° E	0.1148	1.69	0.88
	40° S 70° E	0.1305	1.57	0.86
	60° S 70° E	0.8370	-0.70	0.16
ERA5 from 1991 to 2017	Honnavar	0.0728	-0.17	0.92
	Gopalpur	0.0017	-0.24	0.95
	20° N 70° E	0.0147	-0.22	0.95
	0° N 70° E	0.0524	-0.22	0.94
	20° S 70° E	0.4404	-0.13	0.55
	40° S 70° E	0.1179	-0.48	0.88
	60° S 70° E	0.9333	0.08	0.06
ERA-Interim from 1979 to 2017	Honnavar	0.8088	0.01	0.19
	Gopalpur	0.7074	0.02	0.29
	20° N 70° E	0.1023	0.09	0.89
	0° N 70° E	0.0658	0.10	0.93
	20° S 70° E	0.0050	0.28	0.95
	40° S 70° E	0.1569	0.30	0.84
	60° S 70° E	0.0043	0.79	0.95

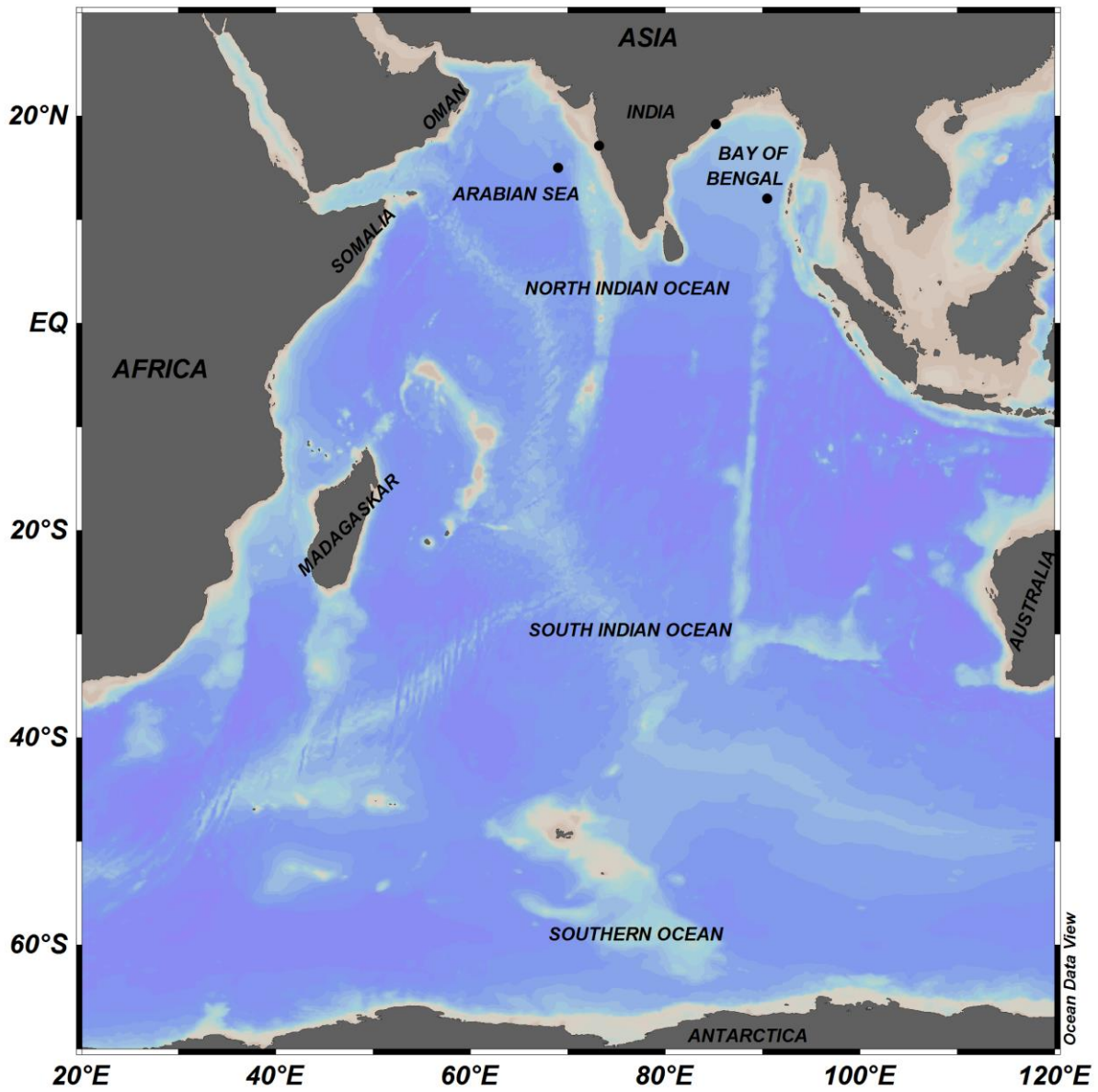


Figure 1. Study area in Indian Ocean with GEBCO bathymetry. Locations of buoy measurements used for ERA5 data validation are denoted by dots

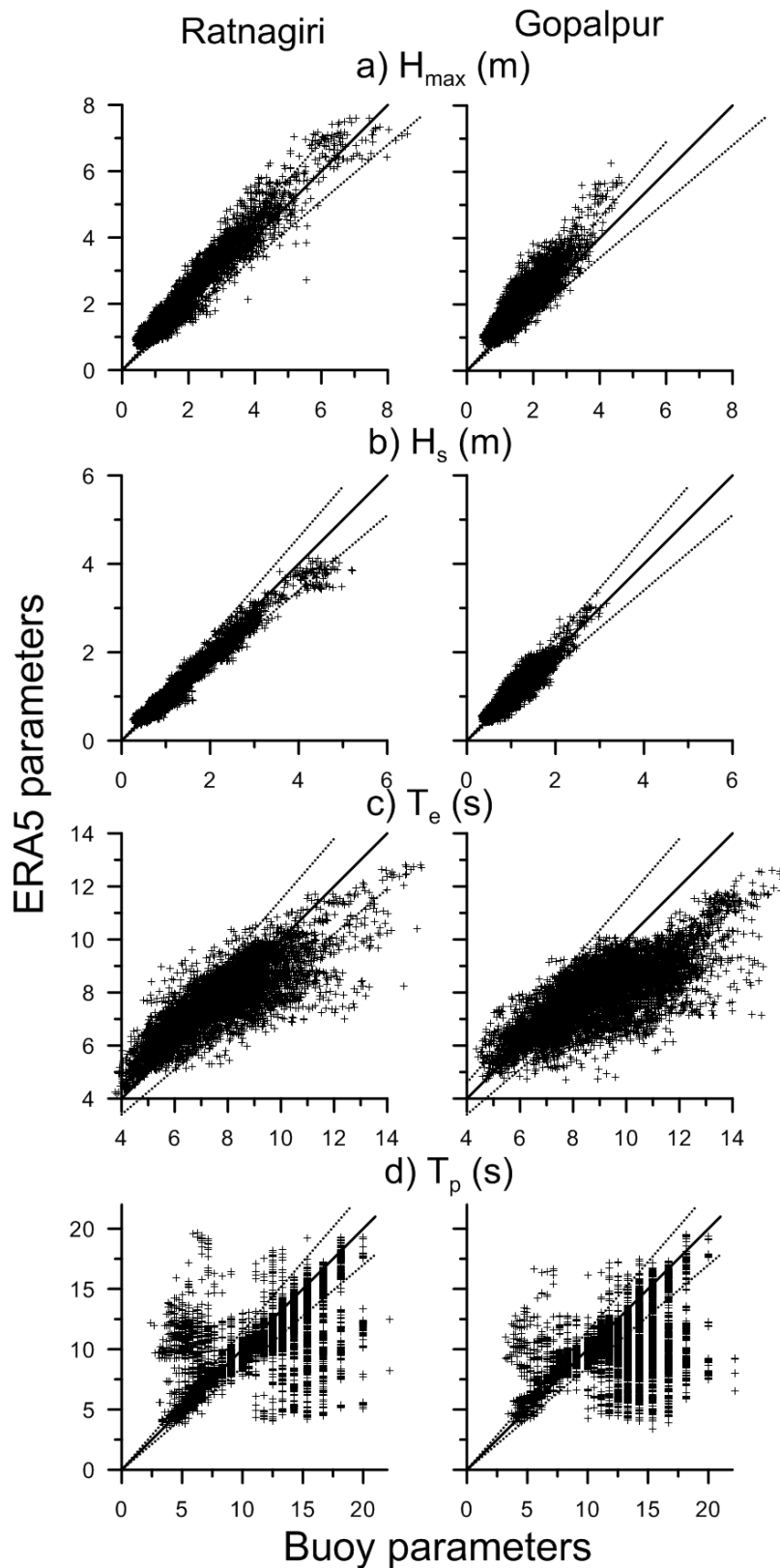


Figure 2. Scatter plots of ERA5 wave data with buoy data a) maximum wave height ( $H_{\max}$ ), b) significant wave height ( $H_s$ ), c) mean wave period ( $T_e$ ) and d) peak wave period ( $T_p$ ). The left panel is for coastal location in eastern Arabian Sea and the right panel is for coastal location in north western Bay of Bengal

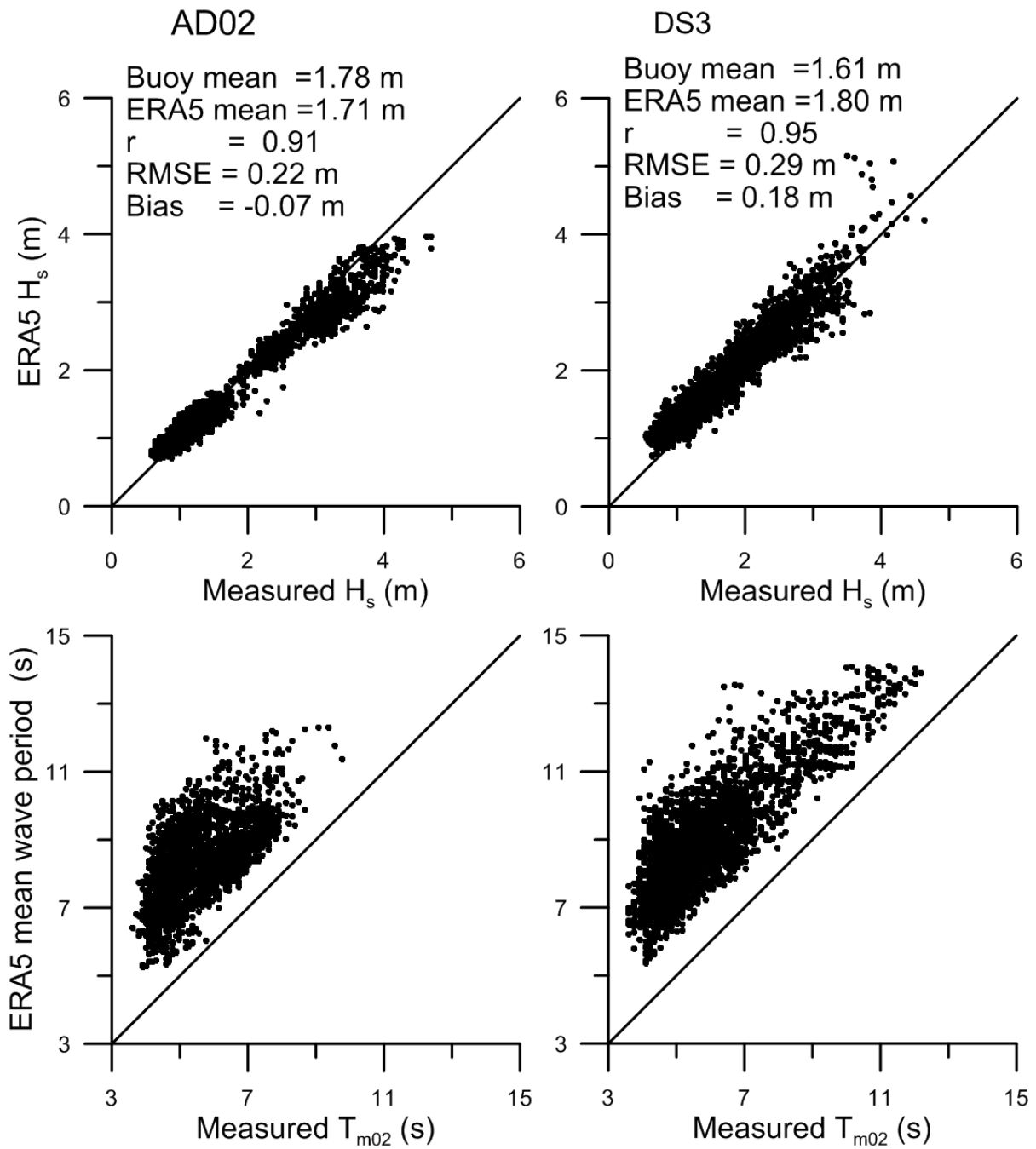


Figure 3. Scatter plots of ERA5 wave data (significant wave height and mean wave period) at deep waters in Arabian Sea (AD02) in 2012 and Bay of Bengal (DS3) in 2003

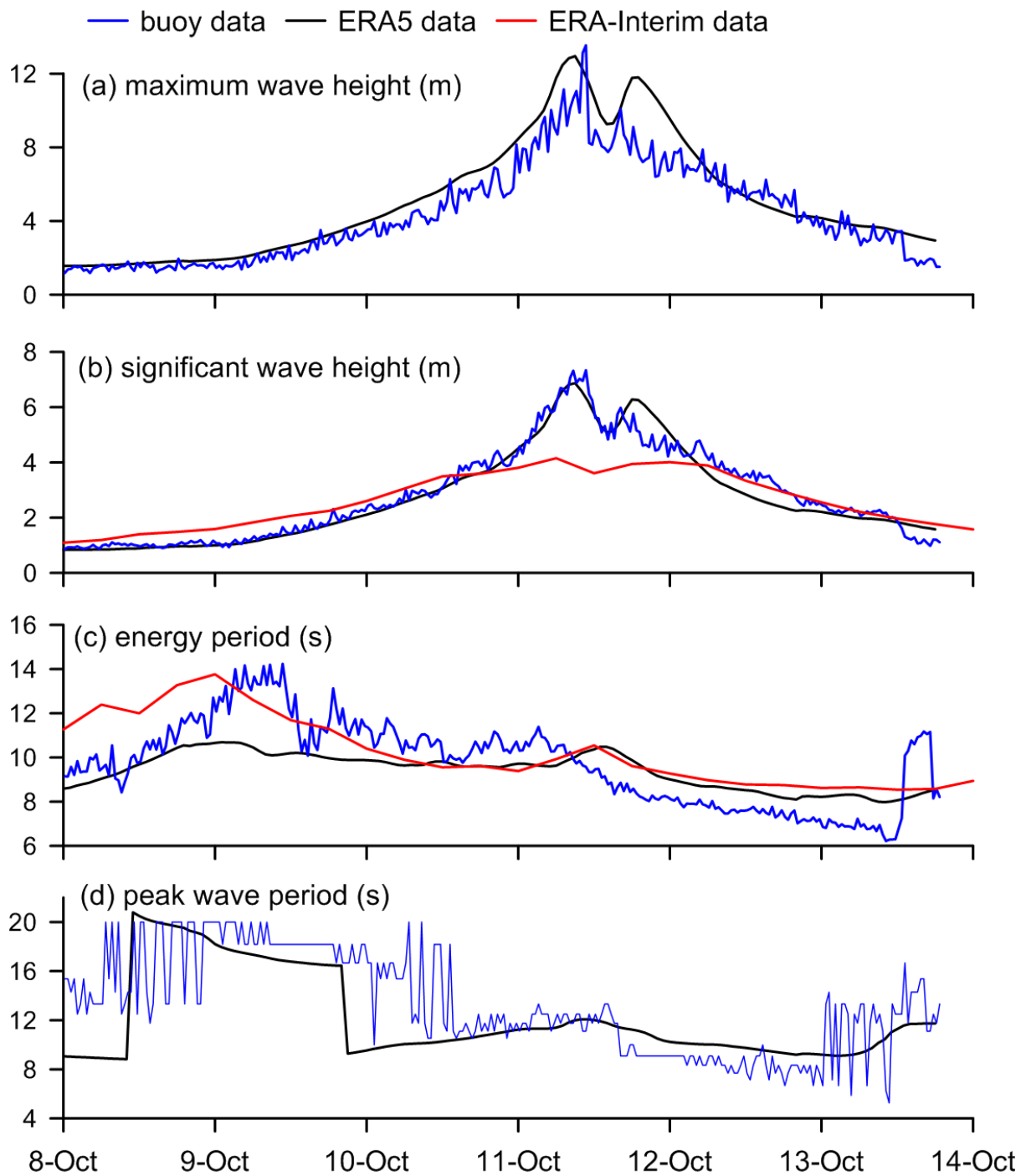


Figure 4. Time series plot of wave parameters from ERA5 and ERA-Interim with buoy measured parameters a) maximum wave height, b) significant wave height, c) mean wave period and d) peak wave period at Gopalpur during tropical cyclone Phailin

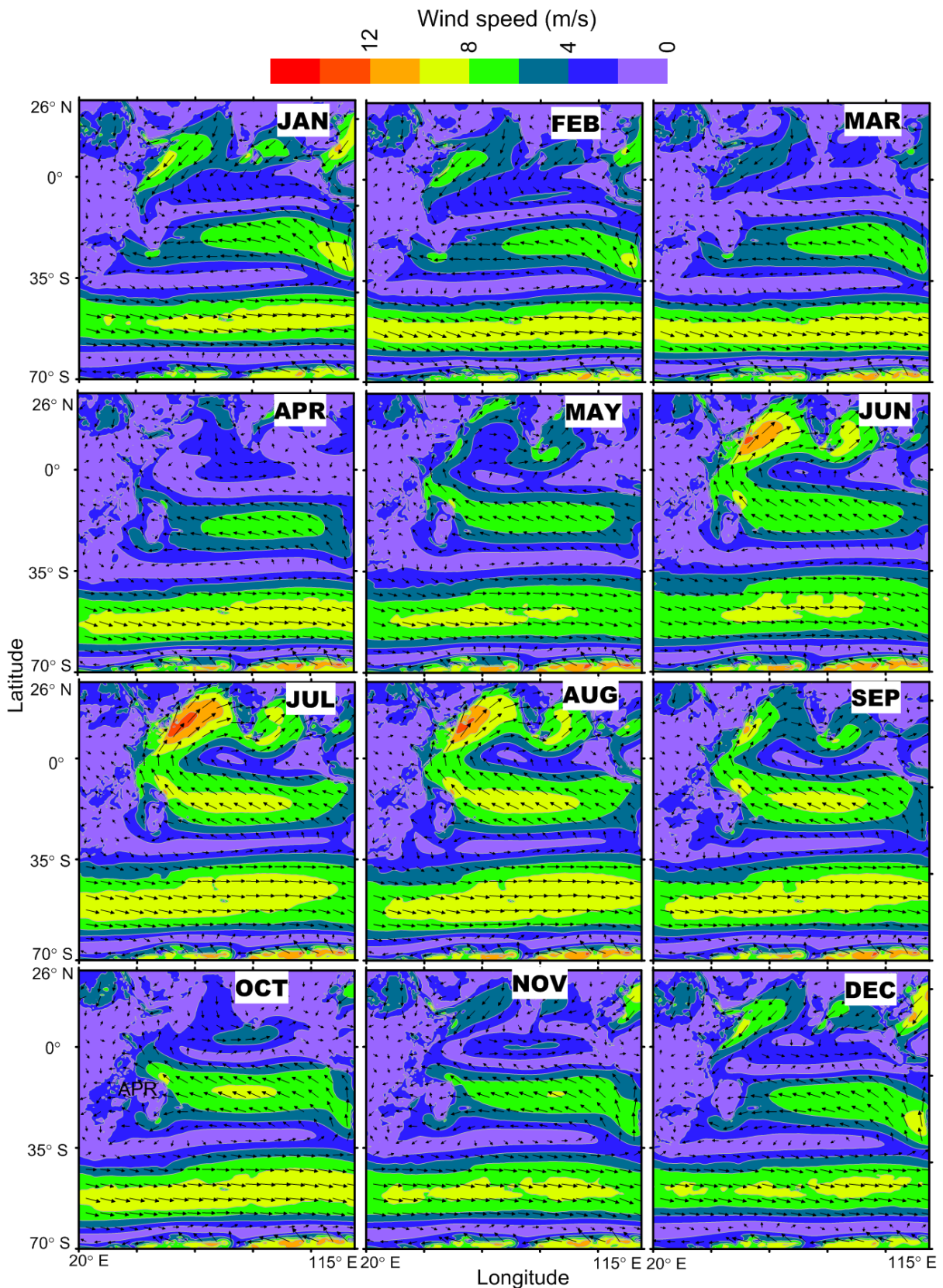


Figure 5. Spatial distribution in monthly averaged wind speed in Indian Ocean from January to December based on data from 1979 to 2017. The colour indicates the wind speed and the arrow show the wind direction

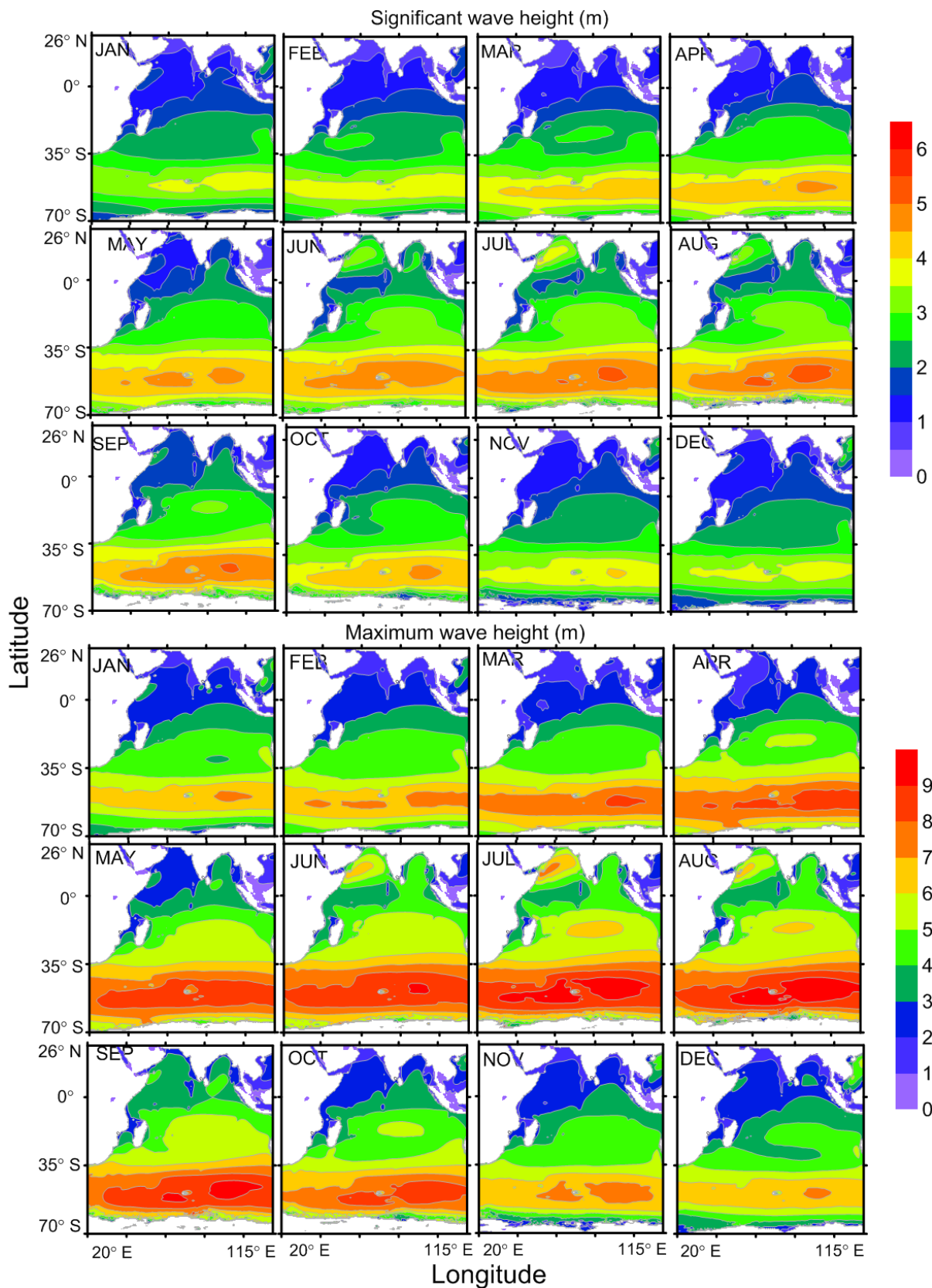


Figure 6. Spatial distribution of monthly averaged a) significant wave height and b) maximum wave height in Indian Ocean from January to December based on data from 1979 to 2017



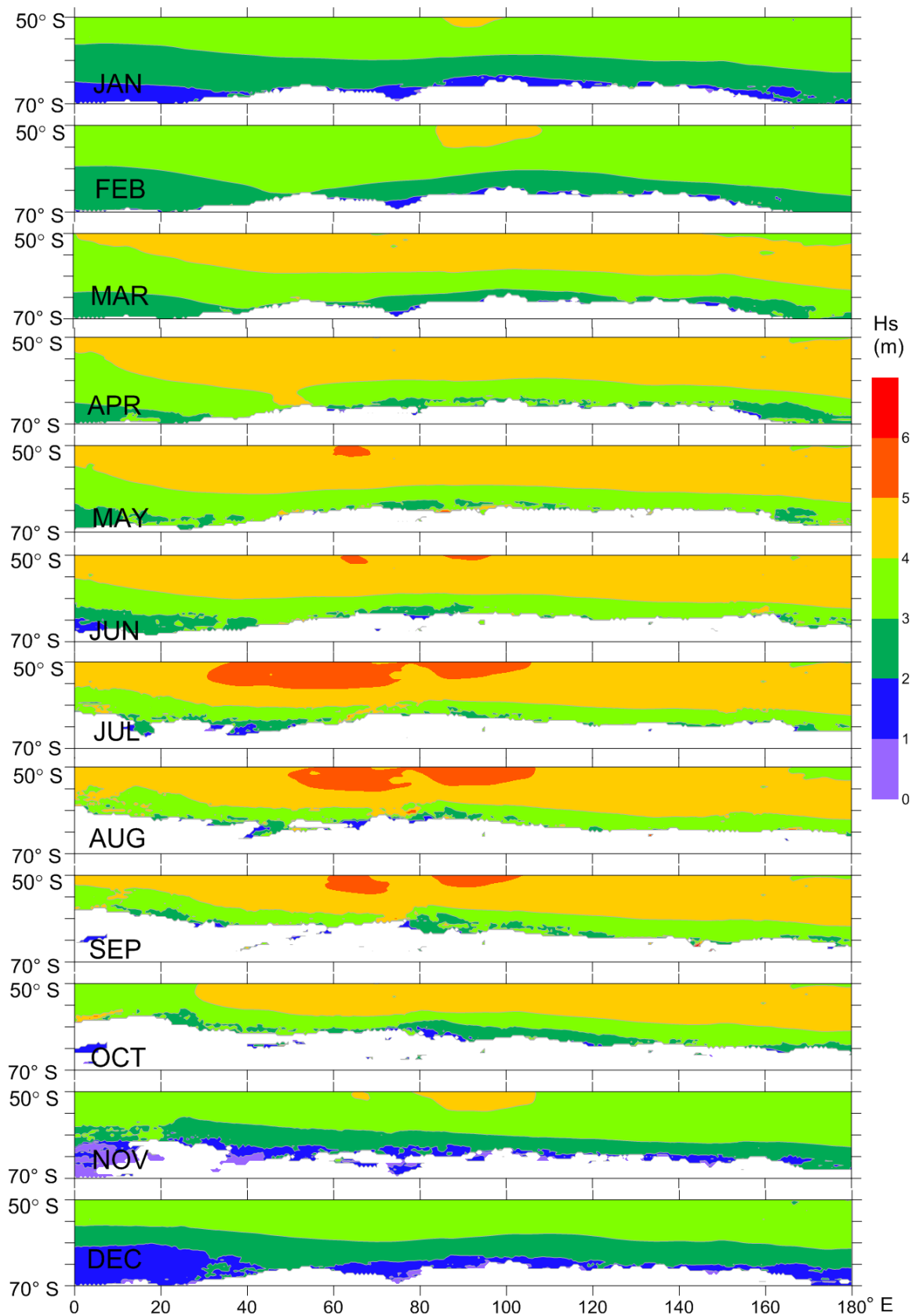


Figure 7. Spatial distribution of monthly averaged significant wave height in Southern Ocean from January to December based on data from 2016 to 2017

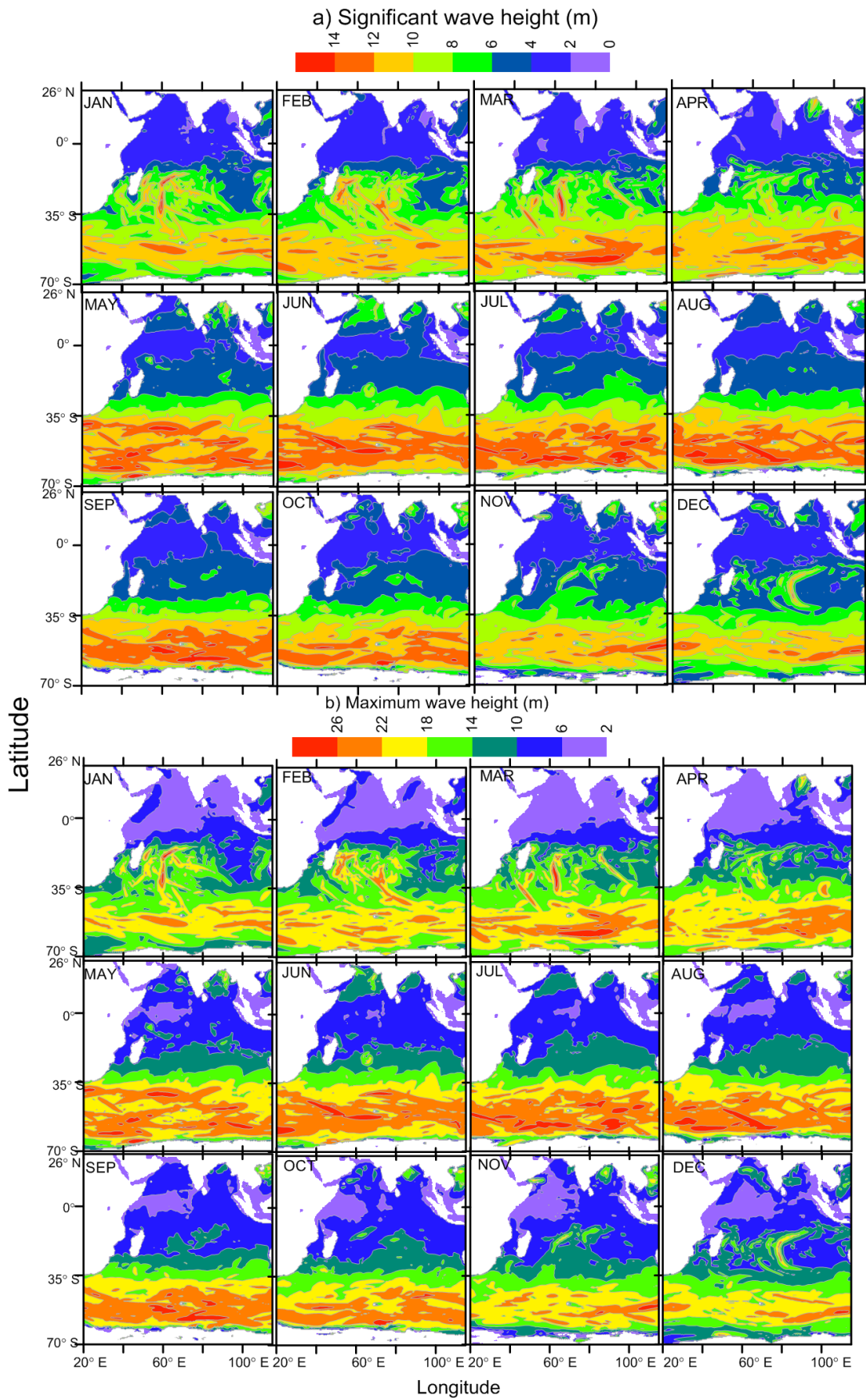


Figure 8. Spatial distribution of monthly maximum a) significant wave height and b) maximum wave height from January to December based on data from 1979 to 2017

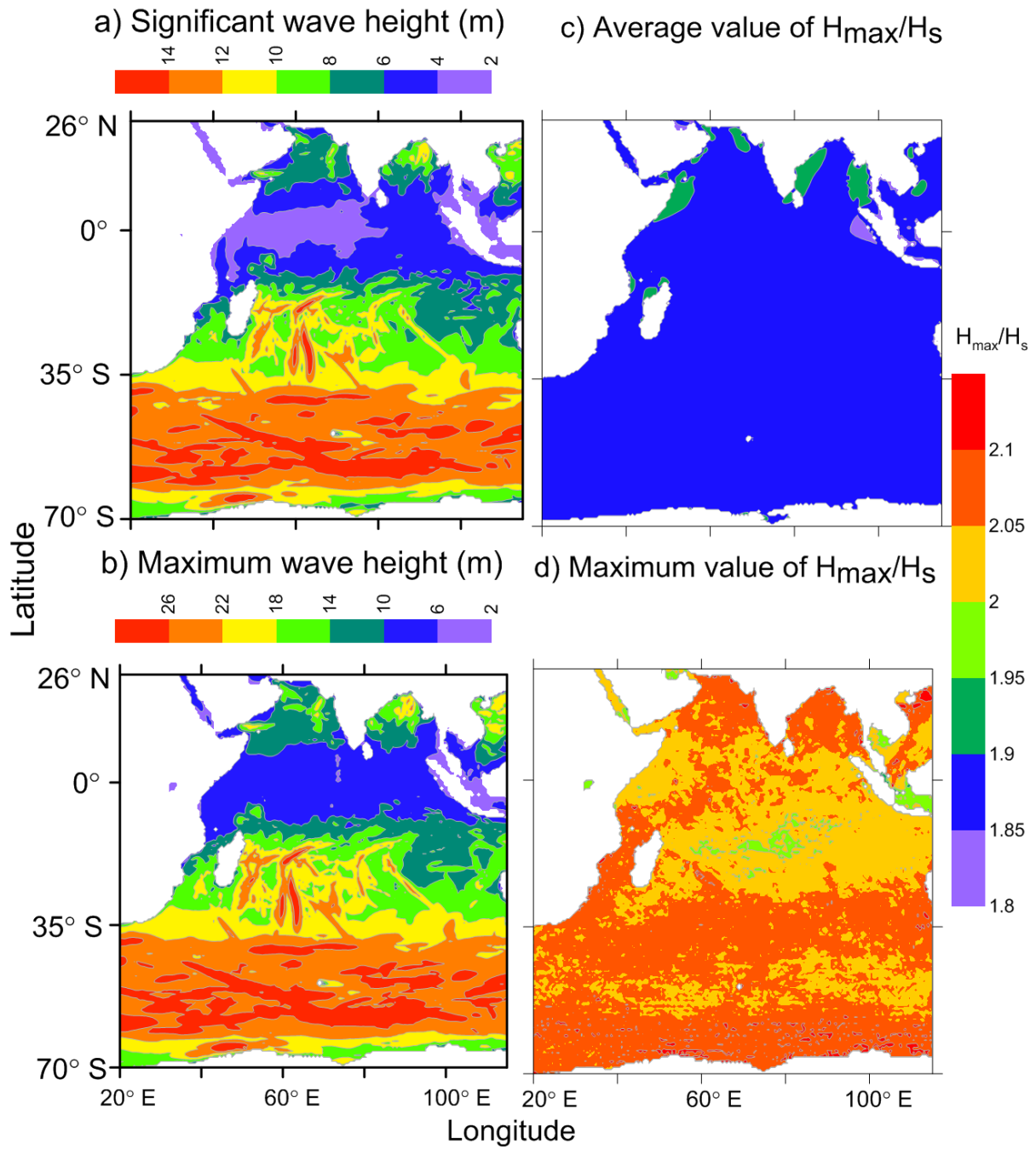


Figure 9. Spatial plot of a) maximum value of significant wave height, b) maximum value of maximum wave height, c) average value of the ratio between maximum wave height and significant wave height and d) maximum value of the ratio between maximum wave height and significant wave height in the Indian Ocean during 1979-2017

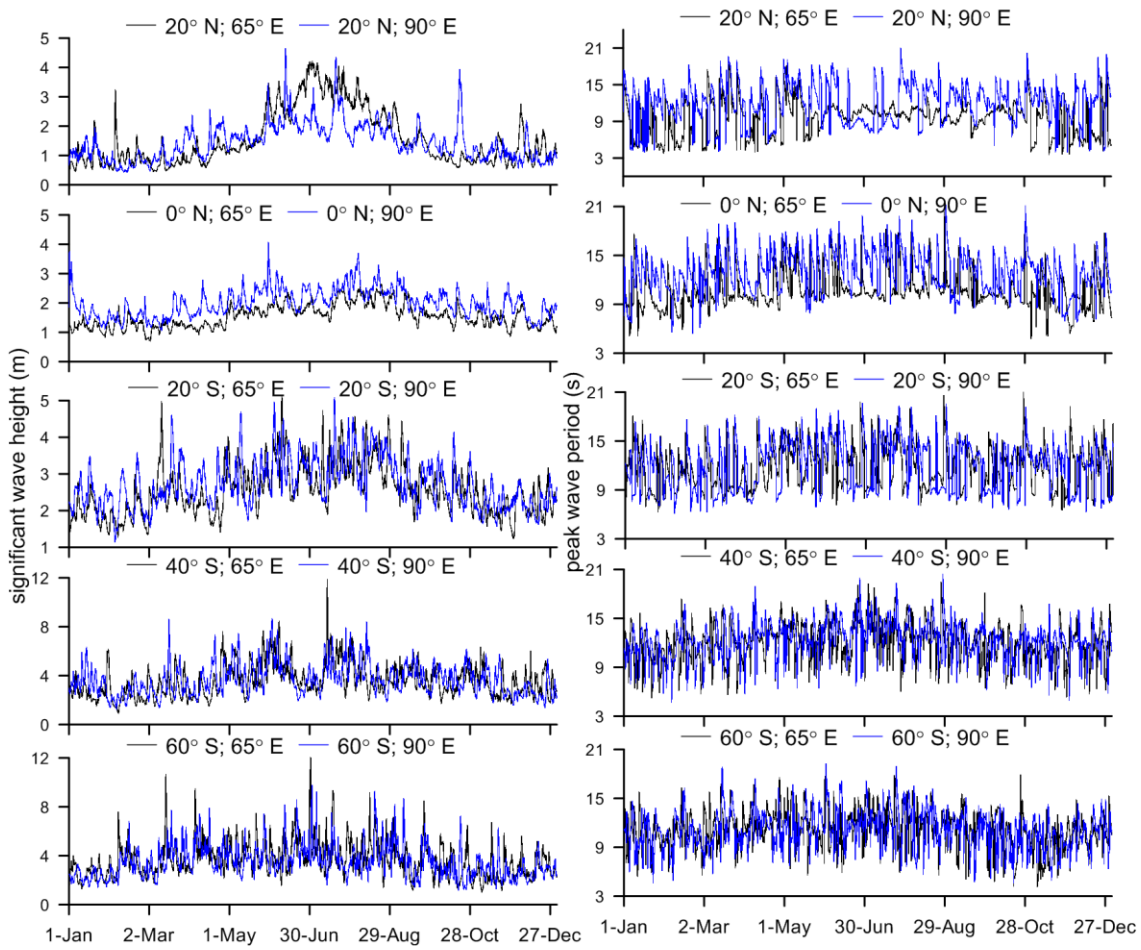


Figure 10. Time series plot of significant wave height (left panel) and peak wave period (right panel) at 5 locations along 65° E and 5 locations along 90° E in 2017

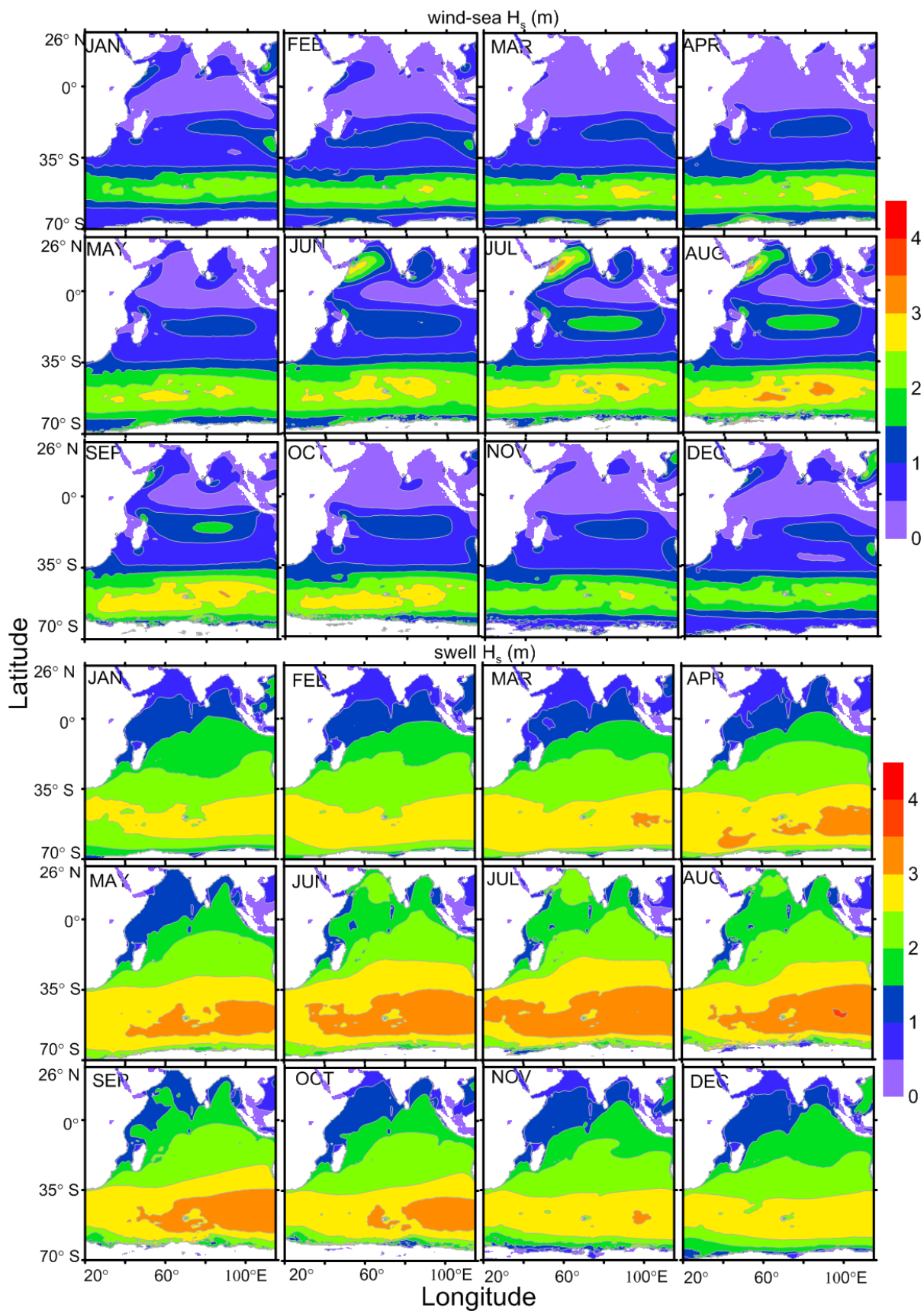


Figure 11. Spatial distribution of monthly averaged a) wind-sea height and b) swell height in Indian Ocean from January to December based on data from 1979 to 2017

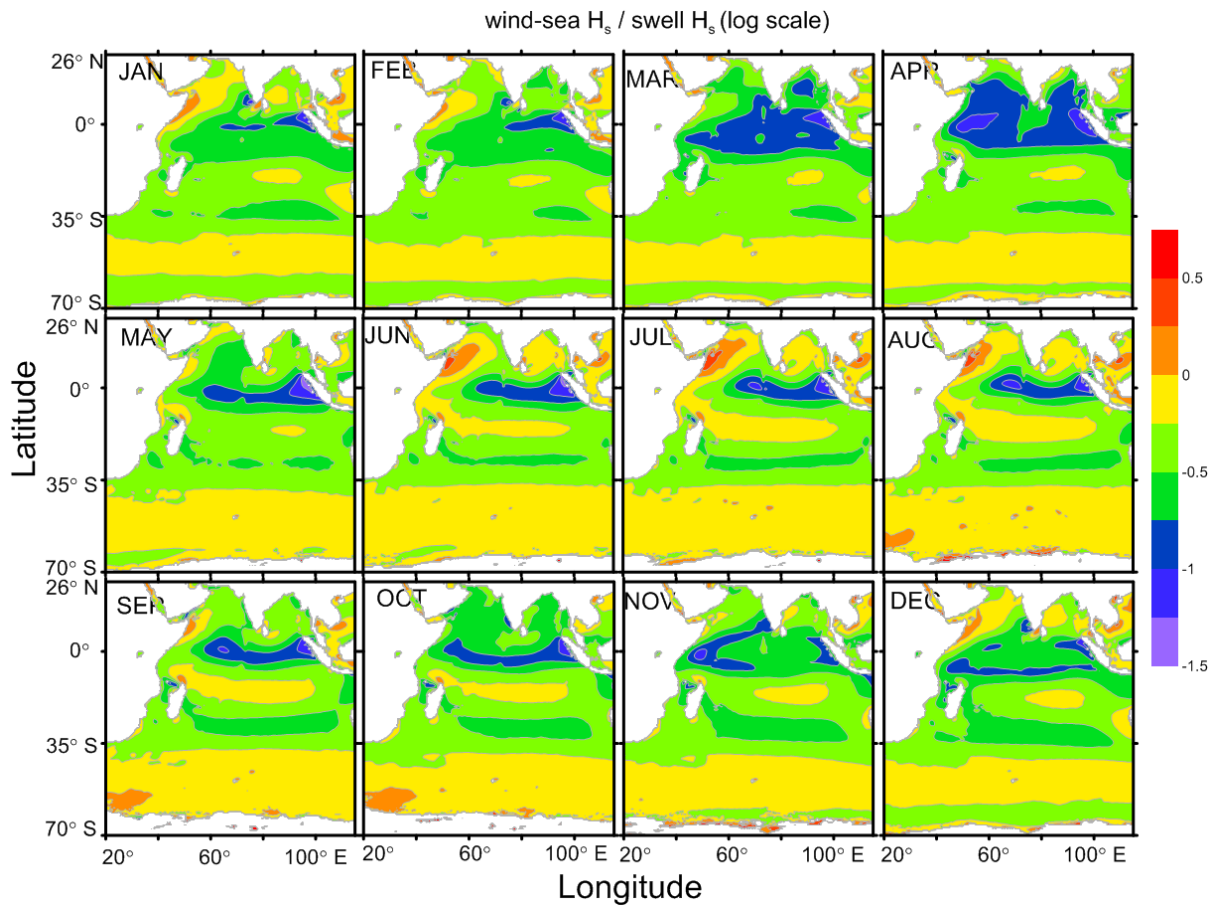


Figure 12. Spatial distribution of the ratio of the wind-sea  $H_s$  to swell  $H_s$ . The contour values are logarithm base 10. Positive values indicate wind-sea  $H_s$  are higher than swell  $H_s$  and negative values are for vice-versa

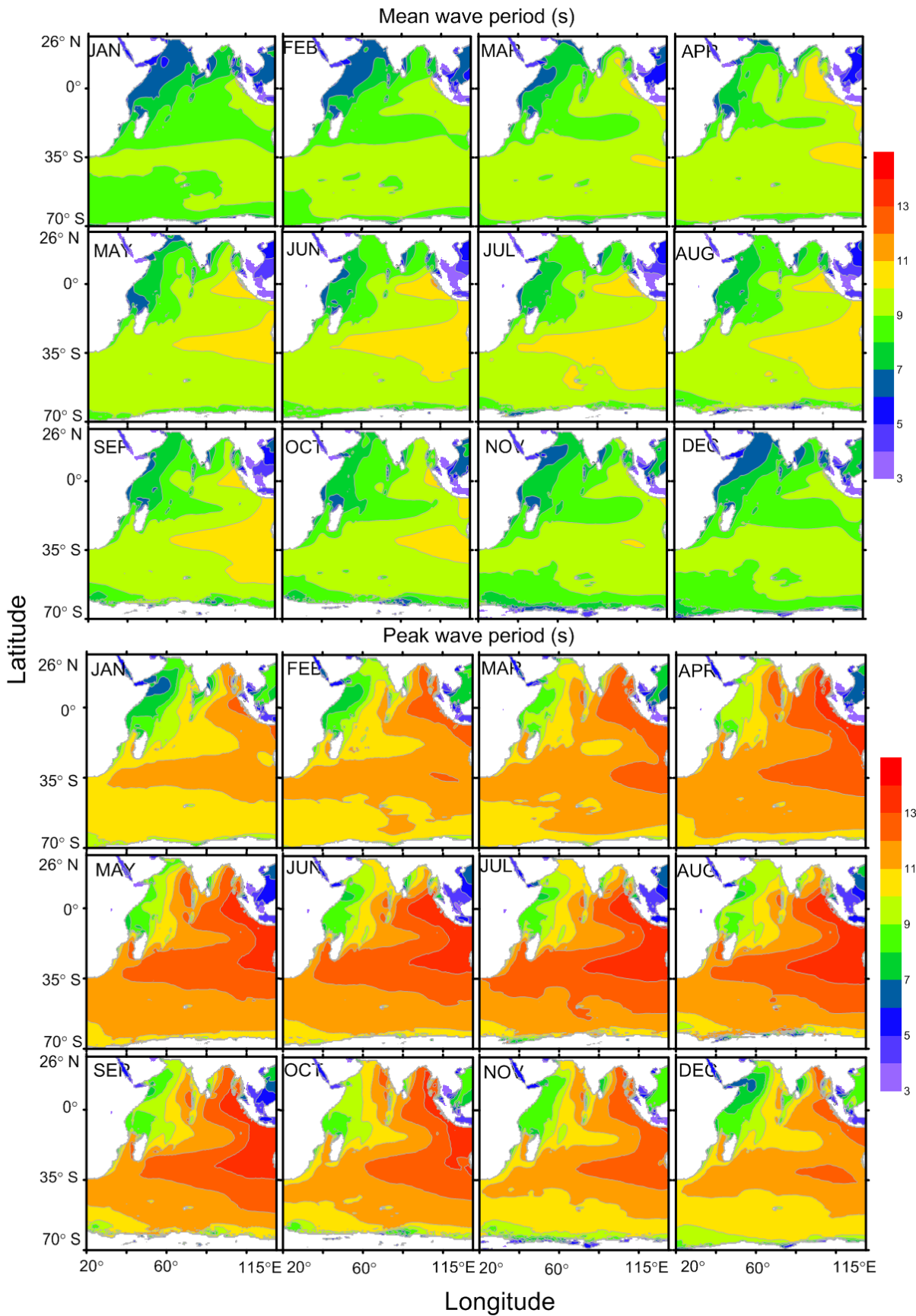


Figure 13. Spatial distribution in monthly averaged a) mean wave period and b) peak wave period in Indian Ocean from January to December based on data from 1979 to 2017

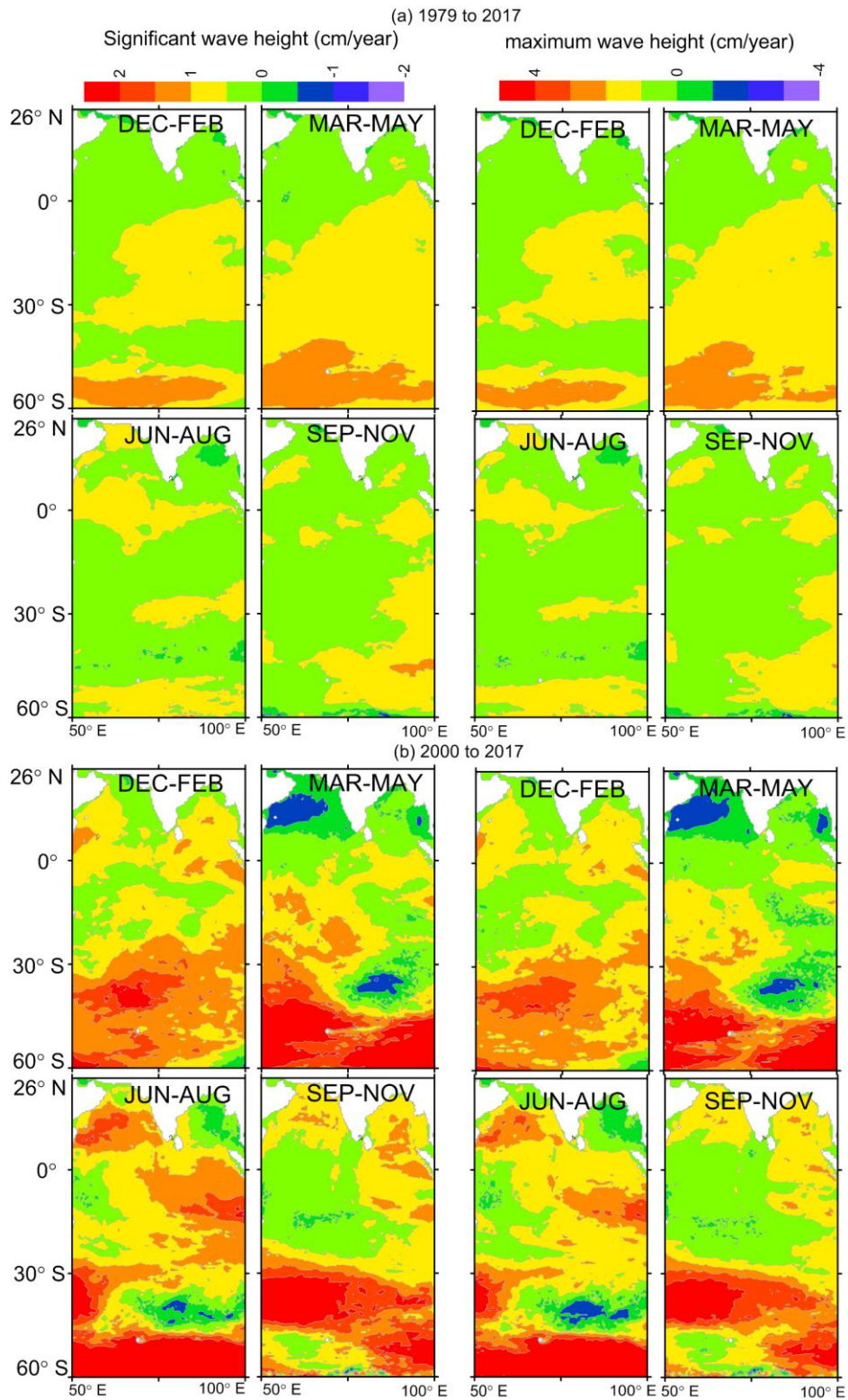


Figure 14. Trend of annual mean wave parameters during a) 1979-2017 and (b) 2000-2017. Left panel is for significant wave height and right panel is for maximum wave height. Sub plots are for different months (December-February, March-May, June-August, September-November)



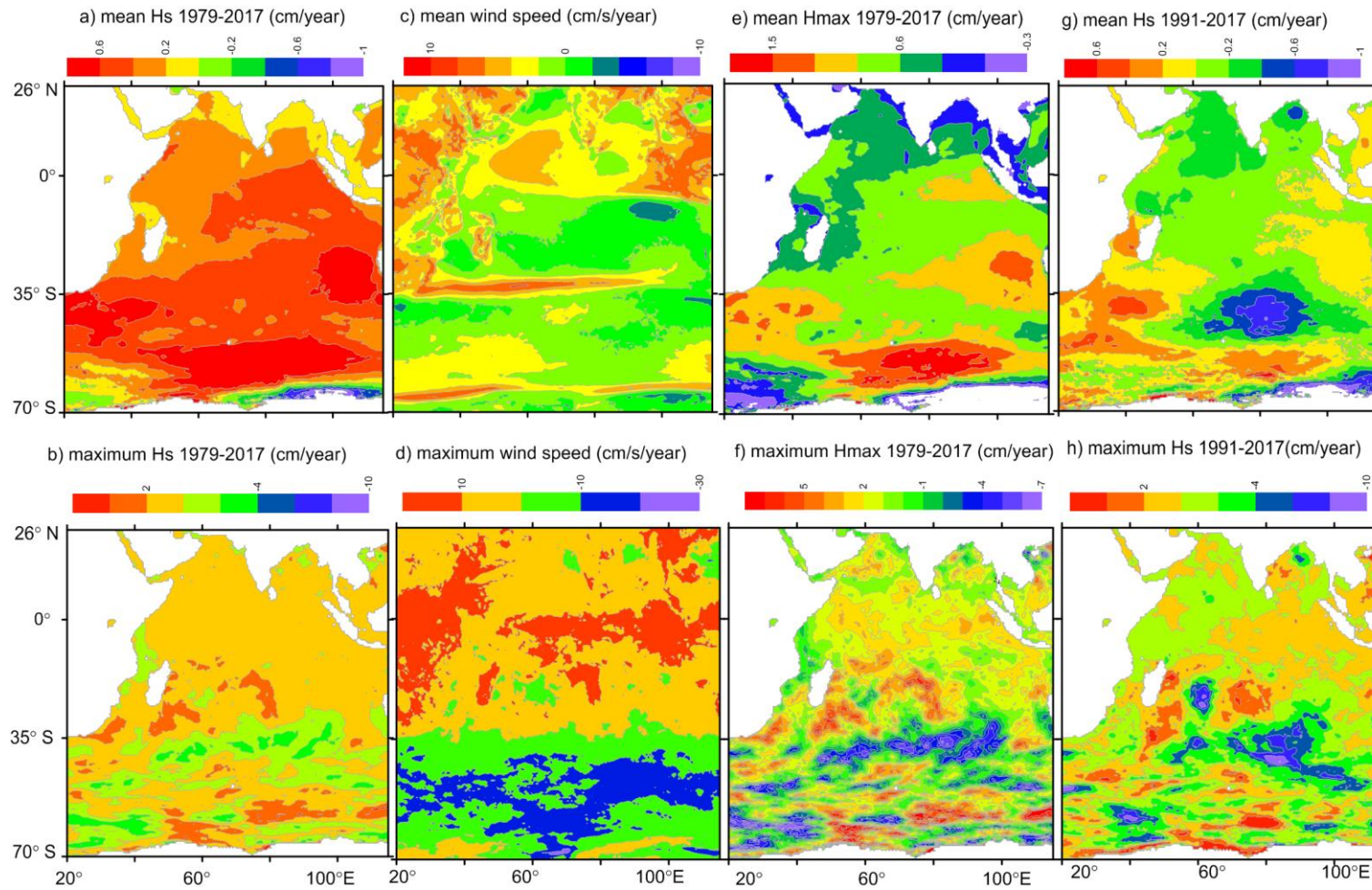


Figure 15. Trend of wind and wave parameters in two different time periods; a) annual mean significant wave height, b) annual mean maximum wave height, c) annual mean wind speed, d) annual maximum wind speed, e) annual maximum significant wave height, f) annual maximum wave height, g) annual mean significant wave height, h) annual maximum significant wave height. a to f are from 1979 to 2017 and g and h are from 1991 to 2017..

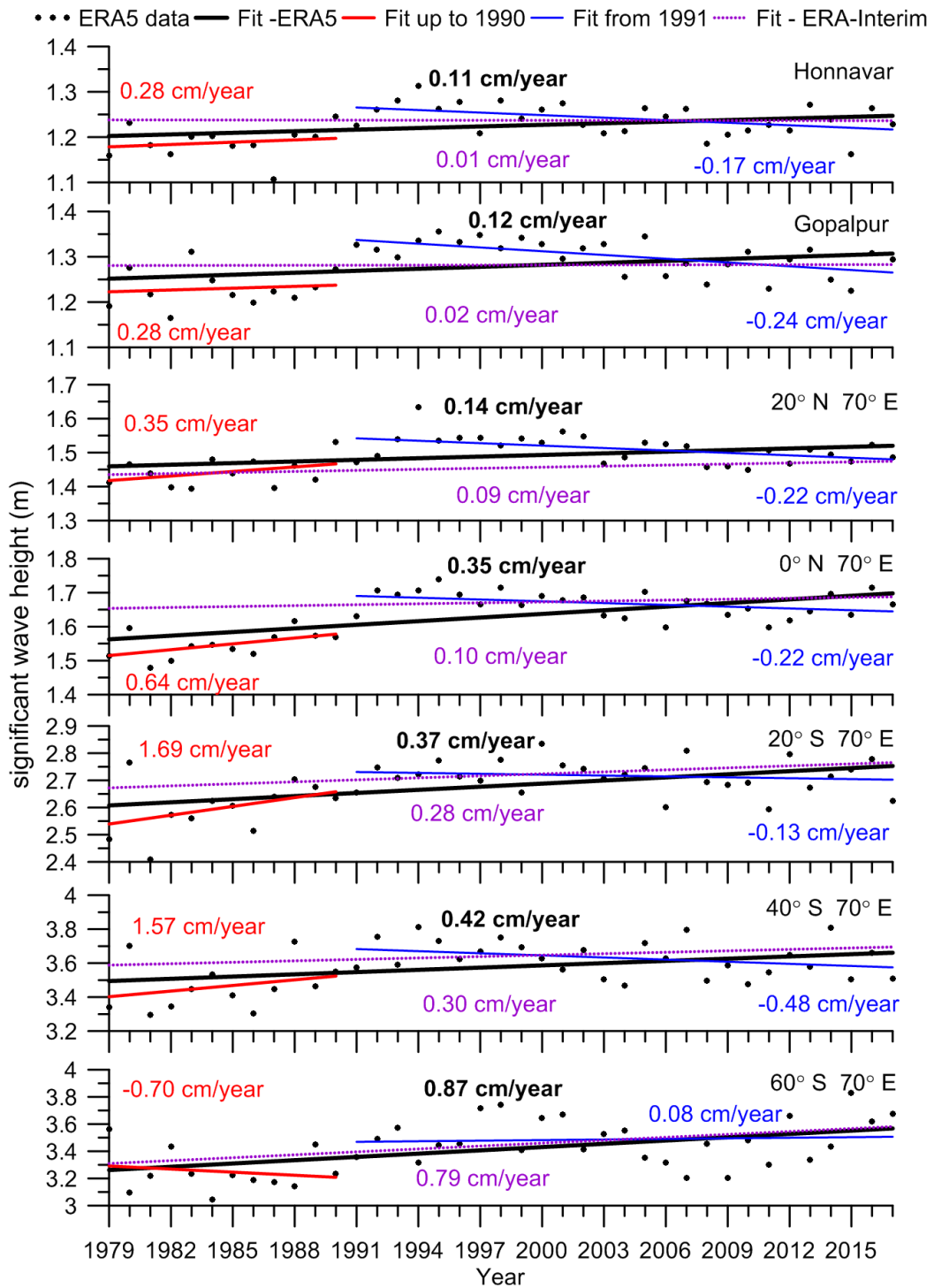


Figure 16. Annual average significant wave height during 1979 to 2017 at two coastal stations and at 5 locations along 70° E. The trend from 1979 to 1990 and 1991 to 2017 are also presented separately. The trend line based on ERA-Interim data is shown in dash line. Trend values are also presented in corresponding colour. The significance and the p value are presented along with trend value in Table 5.

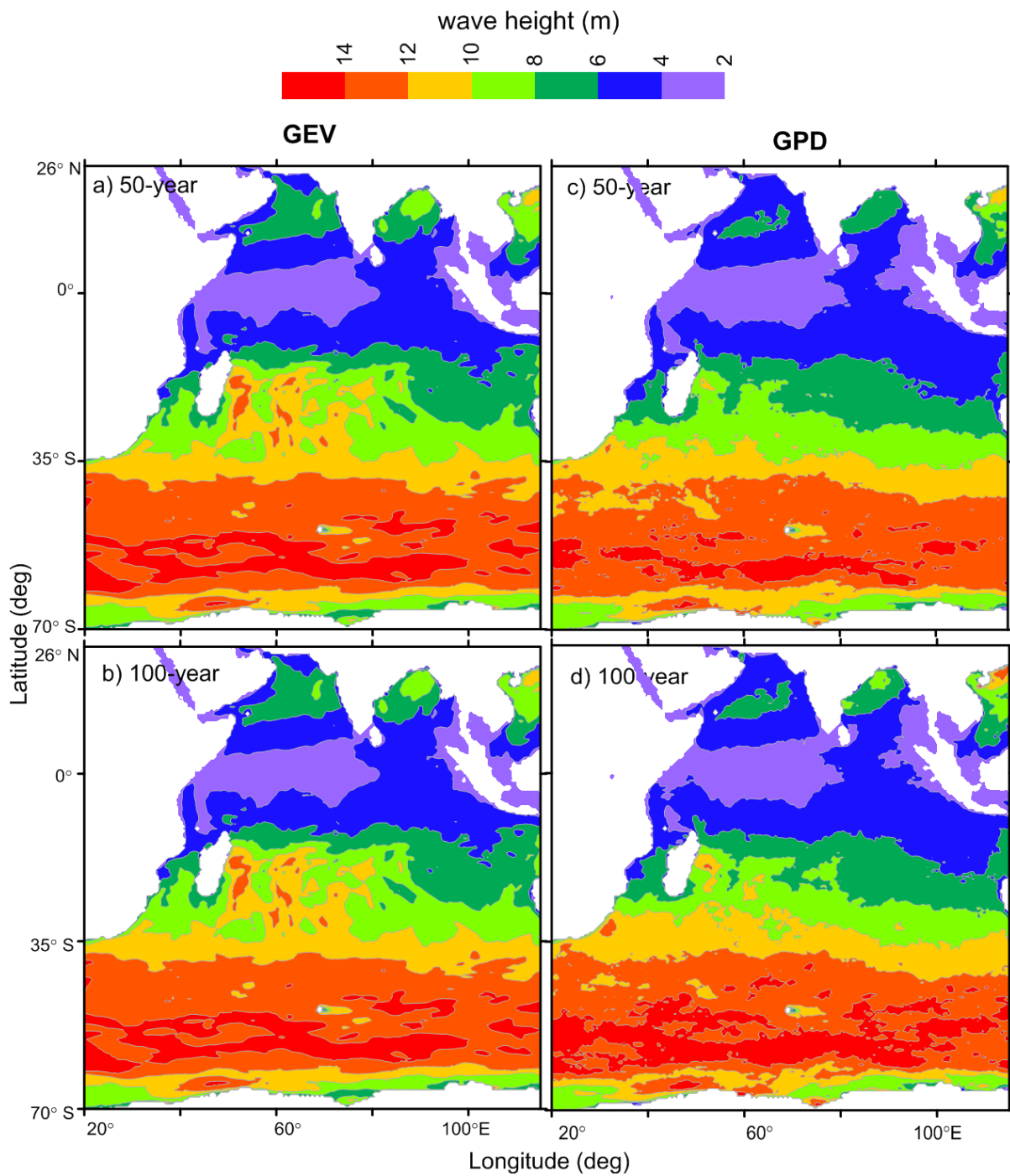


Figure 17. Spatial variation of a) 50-year and b) 100-year return period wave height in Indian Ocean. Left panel is the estimate based on GEV and the right panel is based on GPD

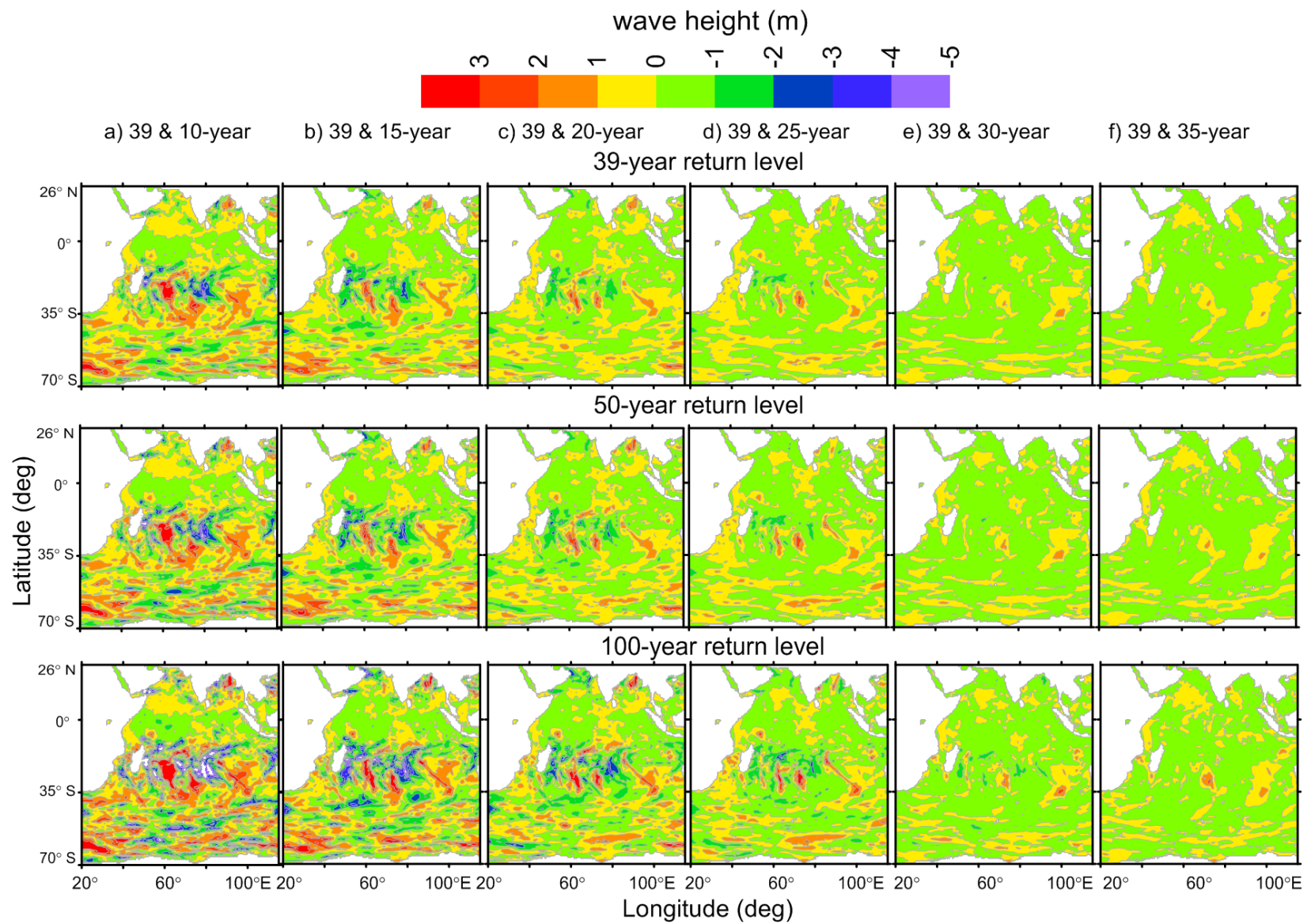


Figure 18. Difference in 39, 50 and 100-year return level in significant wave height for data blocks 10 to 35 years with 39 years